JAEA-Review
2012-047

JAEA-Review

Microstructure Observations and Positron Annihilation Spectroscopic Measurements of ZrC Layers Fabricated by Japan Atomic Energy Agency in Recent R&Ds

Jun AIHARA, Shohei UETA, Masaki MAEKAWA, Atsuo KAWASUSO and Kazuhiro SAWA

Small-sized HTGR Research & Development Division
Nuclear Hydrogen and Heat Application Research Center

February 2013

Japan Atomic Energy Agency

日本原子力研究開発機構

本レポートは独立行政法人日本原子力研究開発機構が不定期に発行する成果報告書です。
本レポートの入手並びに著作権利用に関するお問い合わせは、下記あてにお問い合わせ下さい。
なお、本レポートの全文は日本原子力研究開発機構ホームページ（http://www.jaea.go.jp）
より発信されています。

独立行政法人日本原子力研究開発機構　研究技術情報部　研究技術情報課
〒319-1195　茨城県那珂郡東海村白方白根 2 番地 4
電話 029-282-6387, Fax 029-282-5920, E-mail:ird-support@jaea.go.jp

This report is issued irregularly by Japan Atomic Energy Agency
Inquiries about availability and/or copyright of this report should be addressed to
Intellectual Resources Section, Intellectual Resources Department,
Japan Atomic Energy Agency
2-4 Shirakata Shirane, Tokai-mura, Naka-gun, Ibaraki-ken 319-1195 Japan
Tel +81-29-282-6387, Fax +81-29-282-5920, E-mail:ird-support@jaea.go.jp

JAEA-Review 2012-047

Microstructure Observations and Positron Annihilation Spectroscopic Measurements of ZrC Layers Fabricated by Japan Atomic Energy Agency in Recent R&Ds

Jun AIHARA, Shohei UETA, Masaki MAEKAWA[+1], Atsuo KAWASUSO[+1]

and Kazuhiro SAWA[+2]

Small-sized HTGR Research & Development Division,

Nuclear Hydrogen and Heat Application Research Center,

Japan Atomic Energy Agency,

Oarai-machi, Higashiibaraki-gun, Ibaraki-ken

(Received December 5, 2012)

TRISO coated fuel particle is used in high temperature gas-cooled reactors (HTGRs). SiC has been used as the third layer, the most important coating layer, of TRISO coated fuel particle. On the other hand, zirconium carbide (ZrC) coated fuel particles were fabricated in batch scale of only a few tens of grams, and it was shown that thermal stability of ZrC coated fuel particles was much higher than existing TRISO coated fuel particles, in previous studies. Then from 2004 to 2008, Japan Atomic Energy Agency (JAEA) carried out R&Ds on ZrC coating process with batch scale up to 200 g. In this report, we summarize some characteristics of microstructures and positron annihilation spectroscopy (PAS) of ZrC layers fabricated in R&Ds, in addition to outline of R&Ds process, already published in some papers.

KEYWORDS: High Temperature Gas-cooled Reactor, Coated Fuel Particle, Zirconium Carbide, Microstructure, Positron Annihilation Spectroscopy

---

Present study includes the result of “Research and development for advanced high temperature gas cooled reactor fuels and graphite components” entrusted to the Japan atomic Energy Agency by the Ministry of Education, Culture, Science, and technology of Japan (MEXT).

＋1 Advanced Science Research Center

+2 Department of HTTR

日本原子力研究開発機構における近年のR&Dにおいて製造されたZrC層の微細構造観察と陽電子消滅分光測定

日本原子力研究開発機構　原子力水素・熱利用研究センター　小型高温ガス炉研究開発ユニット

相原　純、植田　祥平、前川　雅樹[+1]、河裾　厚男[+1]、沢　和弘[+2]

(2012 年 12 月 5 日　受理)

高温ガス炉(HTGR)においてはUO_2燃料核をセラミックスで4重に被覆した直径約1 mmのTRISO被覆燃料粒子が使用されている。TRISO被覆燃料粒子において最も重要な被覆層である第3層には現在SiCが使われている。一方、過去の研究において炭化ジルコニウム(ZrC)被覆燃料粒子が数10 gバッチ規模で製造され、更に、既存のTRISO被覆燃料粒子よりも遥かに高い熱安定性を持っていることが示された。そこで2004年から2008年にかけて、(独)日本原子力研究開発機構(JAEA)は200 gバッチまでの規模においてZrC被覆技術開発を行った。本報告は、この技術開発の過程の概要に加え、製造したZrC層の微細構造及び陽電子消滅分光(PAS)の特性についてこれまでに公開してきた成果を纏めたものである。

本報告は、文部科学省からの平成 20 年度エネルギー対策特別会計委託事業により独立行政法人日本原子力研究開発機構が実施した「革新的高温ガス炉燃料・黒鉛に関する技術開発」の成果を含みます。

大洗研究開発センター：〒311-1393　茨城県東茨城郡大洗町成田町 4002

＋1 先端基礎研究センター

+2 高温工学試験研究炉部

Contents

目次

Table list

Figure list

This is a blank page.

1. Introduction

The high-temperature gas-cooled reactor (HTGR) is a type of nuclear reactor that utilizes ceramic-coated UO_2 fuel particles such as tri-structural isotropic or so-called TRISO-coated fuel[1]. A spherical UO_2 kernel is covered with a buffer layer, which is in turn covered with an inner high-density pyrolytic carbon (IPyC) layer. The IPyC layer is again covered with a third layer, for which SiC has been used. The third layer is finally covered with an outer high-density pyrolytic carbon (OPyC) layer. The overall diameter of the TRISO-coated fuel is around 0.9 mm. The materials and roles of each coating layer are described in Table 1.

The very high-temperature gas-cooled reactor (VHTR), a type of HTGR, is one of the most promising candidates for the fourth generation nuclear energy systems[2]. VHTR fuel needs to be designed with excellent safety performance up to burn-up of about 15%–20% fissions per initial metal atom (%FIMA) and fast neutron fluence of 6×10^{25} /m^2 (E > 0.1 MeV). The fuel particles with advanced coating will improve the performance of the VHTR, as they can withstand higher temperatures and higher burn-up than existing TRISO-coated fuel particles.

In studies performed in the early 1970's and 1980's at the Japan Atomic Energy Research Institute (JAERI),which is now Japan Atomic Energy Agency (JAEA), zirconium carbide (ZrC)-coating conditions[3] for obtaining uniform structures and stoichiometry were successfully acquired. This was achieved by using a small-scale coating method involving only a few tens of grams per batch and a ZrC-coated fuel particle, resulting in the successful fabrication of a ZrC coating layer. It should be noted that the coating process is carried out with batch processing system. These studies demonstrated that ZrC-coated fuel particles possess much higher temperature stability than existing TRISO-coated fuel particles[4]. In addition, the ZrC coating layer has been found to have higher resistance to Pd corrosion than a SiC-coating layer[5].

The past studies demonstrated the possibility that ZrC coated fuel particles improve the performance of the VHTR, as mentioned above, however, the batch scale should be enlarged in order that ZrC coated fuel particles are fabricated commercially. Therefore, from 2004 to 2008, the Japan Atomic Energy Agency (JAEA) investigated the following four subjects related to the ZrC coating layer.

(1) Fabrication technology of ZrC coated particles[6-10] with larger batch scale than the past study.
(2) Inspection methods for ZrC-coating[8].
(3) The irradiation effects of ZrC-coated particles[11-13].
(4) Calculation code development for the prediction of failure probability of ZrC coated fuel particles under irradiation[14].

Subject (1) is the most important in the four subjects and the foundation of subjects (2) and (3). Various reports, covering the whole R&D process of subject (1), have been published. Then, in this report, we first summarize outline of subject (1) in some papers[6-10] to report the process and goals of subject (1). Next, we summarize some detailed characteristics of ZrC layers of some important batches[15-18], which were ranked as the milestones in the R&D process.

2. Outline of R&Ds of Fabrication Technology of ZrC Coated Particles

The most important target of this R&Ds was to develop the fabrication technology of ZrC coated particles with reduced excess carbon with larger batch scale than the past study. Too much excess carbon adversely affects the performance of the ZrC coating layers[19,20]. In addition, ZrC-OPyC continuous coating was another target of the R&Ds. The failure of the coating layers with handling can be avoided with continuous coating.

2.1 Coating Procedure

2.1.1 Feed Particles

The feed particles with a diameter of approximately 0.8 mm were spherical inner high density pyrolytic carbon (IPyC)-coated stabilized zirconia with a diameter of approximately 0.72 mm[15-17]. The surface of the feed particles was high density pyrolytic carbon (PyC, because the ZrC layer needs to be coated on PyC in a practical process for the fuel particles. The diameter of the zirconia and the thickness of the IPyC layer were set to match those of particles with UO_2 kernels to be deposited with ZrC layers[15-17]. This was because the state of fluidization depends on the weight and diameter of the particles. As well as this, UO_2 kernels are isolated from the material gas of ZrC with an IPyC layer, and as such, the state of deposition obtained is transferable to a real UO_2 system.

2.1.2 Chemical Process[9]

In the previous study at the JAERI, some coating techniques of ZrC have been examined by the chemical vapor deposition (CVD) using zirconium halide vapors such as iodide, chloride and bromide in laboratory scale[3]. Then, it was found that the bromide process was preferred to other halide processes experimentally, because it was easier to produce the stoichiometric composition of ZrC.

In the bromide process, the ZrC-coating layer is deposited with pyrolytic reaction of zirconium bromide, CH_4 and H_2 in a fluidizing bed. Main reactions of the bromide process can be described as follows[3]:

$$[CH_4] = (C) + 2[H_2] \quad (1)$$

$$[ZrB\ r_4] + [H_2] \rightarrow [ZrBr_3], [ZrBr_2] + [HBr] \quad (2)$$

$$[ZrBr_x] + (C) = (ZrC) + x[Br]\ (x=2,3,\text{or } 4) \quad (3)$$

$$[Br] + (1/2)[H_2] = [HBr] \quad (4)$$

$$(1/4)\ (C) + [HBr] = (1/4)\ [CH_4] + [Br] \quad (5)$$

In cases of ZrC-OPyC continuous coatings, the OPyC layer is deposited with pyrolytic reaction of propylene continuously after the ZrC deposition[7].

2.1.3 Coating Equipment[9]

A new ZrC coater was constructed at Oarai Research and Development Center of JAEA as shown in Fig. 1. The ZrC coater was designed with the maximum batch size of 200 g, which is about ten times larger than the previous one in the JAERI.

The ZrC coater mainly consists of the gas supply equipment, the CVD coater, and the off-gas combustion equipment. At the gas supply system, liquid bromine is vaporized with argon as carrier gas at the temperature of 0 ^{o}C, and the bromine gas is introduced into the CVD coater from the bottom. The mixed gas with methane and hydrogen is also transferred into the coater. The CVD coater is composed of the lower and the upper heaters with in-line configuration to motivate ZrC reaction described in Eqs.(1)-(5). The introduced bromine gas reacts with metallic zirconium sponge loaded in the lower heater, and then produces Zirconium bromide gases at about 873 K. The upper heater has a particle fluidizing bed, and ZrC is coated on the surface of the particle. The particles are heated with a high-frequency coil. The off-gas treatment equipment treats soot, hydrogen bromide and hydrogen.

2.2 Outline of R&Ds Process

At the beginning of the R&Ds[9,18], ZrC coating temperatures were controlled by the feed-back control of the power of high-frequency coil. Then the coating temperature was oscillated in the range of 150 K with time cycles of 5 minutes or less. Then the circumferential stripes reflecting its un-uniform microstructure were observed in the ZrC layer. ZrC layer of a batch fabricated in this step was observed in detail, to clarify the effect of the oscillation of the coating temperature on the microstructure of the ZrC layer (see subsec. 3.3.1).

In the next step, the control method of power of high-frequency coil was changed into fixed-power, and then the ZrC layers with uniform microstructure were fabricated[8]. In this step, the particle inventory was fixed to be 50 g and the material gas flow rates were fixed,

and then ZrC deposition tests were carried out at various coating temperatures to find the coating temperature for less excess carbon[6,8]. The microstructures of the ZrC layers fabricated in this step, including much excess carbon, were observed with TEM and STEM in detail[15,16], to obtain the knowledge on the microstructure of excess carbons in ZrC layers and the effects of heat treatment on the excess carbons (see subsec. 3.3.2).

After the searching the deposition temperature for ZrC layer with less excess carbon, batch scale was increased up to 100 g, and the material gas flow rates were optimized, and then near stoichiometric ZrC layers were deposited in 100 g batch scale[6,8,12].

With increasing batch scale, "white powder problem" arose[6]. The white powder, which was considered to be $ZrBr_4$, was produced during the coating process. More white powder was produced as batch scale became larger or thicker ZrC layers were deposited, then the exhaust pipe of the coater was stopped up with the white powder[6]. We resolved that problem as follows[6];

- A space was installed for the trapping the white powder, as shown in Fig. 2.
- A system for the depressurization in an emergency before the heaters of the coater was added, as shown in Fig. 3.

In addition, it was clarified that ZrC was deposited not only on the particles but also on the inner surface of the nozzle of the spout bed, and the inner diameter of the nozzle was decreased with the deposited ZrC[6]. The deposition rates at the nozzle were increased with the temperature at the nozzle. Then the coating temperature should be set in order that the temperature at the nozzle is enough low, to avoid the harmful decrease in the inner diameter of the nozzle. If the inner diameter of the nozzle is too small, the particles cannot be spouted. The maximum permissible temperature at the nozzle would depend on the initial inner diameter of the nozzle, batch scale and the deposition duration.

Then ZrC-OPyC continuous coating tests were carried out, after searching deposition temperature for OPyC layers with adequate density by only-PyC coating tests[7]. It should be noted that failure of the coating layers with handling can be avoided with continuous coating, as mentioned above. We have succeeded to coat continuously the near stoichiometric ZrC layer and the OPyC layer with the thicknesses up to about 27 and about 48 μm, respectively, in the batch scale of 100 g[7]. The coated particles with near stoichiometric ZrC and OPyC layers are a goal in this R&Ds, as mentioned at the beginning of this chapter. The microstructures of the ZrC layers fabricated in this step were observed with TEM and STEM in detail[17] before and after heat treatment, to obtain the knowledge on the microstructure of the near stoichiometric ZrC layers(see subsec. 3.3.3). It should be noted that the practical ZrC layers will be near stoichiometric.

As mentioned later (see subsec. 3.3.3), the microstructural observations clarified the remained problem of quality of fabricated ZrC layers, then positron annihilation spectroscopic

(PAS) measurements of various ZrC layers were carried out, because the remained problem seemed to be related to vacancy defects in the ZrC layers, as mentioned layer (see sec. 3.4).

In the last stage of the R&Ds, batch scale was increased step by step, and then the ZrC layers were deposited in 200 g batch scale[10]. The ZrC coated particles in 200 g batch scale are another goal in this R&Ds, as mentioned at the beginning of this chapter.

3. Microstructure Observations and PAS Measurements of ZrC Layers

3.1 Basic Data of Specimens

Basic data on coated particles for each batch reported in this paper are shown in Table 2, with the summary of detailed characterization mentioned in secs. 3.3 and 3.4. Coating procedures are described in the previous chapter.

The coated particles in batches other than batches D and I were annealed to study the effects of the fuel compact sintering process on microstructure evolution in the particles[16,17]. The heat treatment condition was set so as to simulate the thermal history of the fuel compact sintering process for the High Temperature Engineering Test Reactor (HTTR) at JAEA. First, the coated particles were heated in a vacuum at a rate of about 200 K/min. They were then kept at 2033 K for 1 h, before finally being cooled to room temperature (RT) at a cooling rate of about 140 K/min.

3.2 Methods

3.2.1 Microstructural Observation[15-18]

Cross-sectional TEM specimens of the ZrC layers were prepared by a focused ion beam (FIB) micro sampling method using FB-2000A (Hitachi Co. Ltd) with 30 kV Ga ions. The preparation was made without resin embedding for the polished cross section of the particles.

TEM observations were carried out at RT using HF-2000 (Hitachi, Co. Ltd.) and JEM-2000FX for batch I and other batches, respectively. STEM observations were carried out at RT using HD-2000 (Hitachi Co. Ltd.).

In scanning electron microscope (SEM) observation, coated particles were mechanically crushed, and fractures in the coating layers were observed using S-3000N (Hitachi Co. Ltd, Tokyo, Japan) at RT.

3.2.2 PAS Measurements[17)]

A positron microbeam with a diameter of 10 μm and energy of 20 keV was generated using an apparatus based on a commercial SEM system featuring a ^{22}Na source and a solid neon moderator. The details of the apparatus were as described elsewhere[21-23)]. To evaluate the quality of the ZrC layers, OPyC layers were removed from all particle specimens. The positron microbeam was then aimed at the ZrC layers. The average implantation depth of positrons was estimated to be 0.8 μm. Doppler broadening of annihilation radiation (DBAR) measurements was carried out using a high-purity Ge detector with an energy resolution of 1.4 keV at 511 keV. DBAR spectra were characterized by S and W parameters, defined as the spectrum peak and tail area intensities, respectively. These energy windows were 510.19-511.8 and 512.28-519.52 keV. Powdered ZrC with a purity of 99 % and an average particle size of 45 μm was used as a reference specimen. All the S and W parameters were normalized to those obtained for the powder specimen.

3.3 Results and Discussion

3.3.1 ZrC Layer Fabricated at the Beginning of R&Ds (Batch I)[18)]

Dark-layered-structures, which elongated directions were roughly perpendicular to the growth direction, were observed in a HAADF (high angle annular dark field) image (see Fig. 4(a)). Although, the dark-layered contrasts are not distributed uniformly, densely and thinly assembled regions are layered roughly normal to the growth direction. It appears that the stripes observed on the optical microscopic image reflects the non-uniform distribution of the dark layered structure.

It seems quite reasonable to conclude that the dark contrasts appeared in the HAADF image of the layered structure indicate that the average atomic number in the region was smaller than that in the surrounding area. The EDX/STEM spectra showed that the ratio of C peak to Zr peak is remarkably higher in the dark layered structure than in the surrounding area. In addition, lattice fringes like carbon nanotubes[24)] were observed in the above mentioned layered structure in a high resolution TEM image (see Fig. 4(b)). Therefore, we can conclude that the layered structures are those consisting of free carbon.

The free carbon regions were lengthened mainly along the circumferential direction, winding rectilinearly, and around 10 nm in width (see Fig. 4(a)). The fringes observed in the free carbon region were also winding rectilinearly along with the free carbon region as seen in Fig. 4(b). It is most probable, therefore, that the structure of the free carbon region is such that c-plane is roughly parallel to its lengthened direction. The oscillated deposition temperature can result in non-uniform distribution of the free carbon region because the

stoichiometry of ZrC layer depends on the deposition temperature[3]. Accordingly, it is important to improve the quality of ZrC coating layer to keep the deposition temperature constant at an appropriate one.

In addition, the Br peak was detected only in the free carbon region, showing that Br was segregated in the free carbon region.

3.3.2 ZrC Layer with Much Excess Carbon (Batch A)

(1) Before Heat Treatment[15]

A number of laminar features were found by their bright contrast in a bright-field TEM image (Fig. 5(a)). These appeared to be lattice fringes, similar to the free carbon region observed in the ZrC layer of batch I, as shown in the previous section. It is therefore reasonable to assume that these laminar features consisted of mainly free carbon. The free carbon regions were distributed in the ZrC layer uniformly (in micrometer order) and quite densely (Fig. 5(a)), reflecting the large C/Zr value (1.35) of this batch. The elongated direction of the free carbon regions was undulated, as can be seen in Fig. 5(a), which showed that the ZrC layer was deposited unevenly, resulting in a surface with no gloss.

It can be seen that the ZrC layer was bound to the IPyC layer (Fig. 5(b)). The “fibrous carbons” were formed on the IPyC/ZrC boundary and around the pores existing near the boundary, as can be seen in Fig. 5(b). This structure would be turbostratic[25] and corresponds to the “tangled or fibrous structure” described in Pollmann et al.[26].

(2) After Heat Treatment[16]

Figures 6(a) and (b) show the HAADF images including the IPyC/ZrC boundary of the TEM specimens before and after heat treatment, respectively. The dark contrast areas seen in the ZrC layers correspond to voids or free carbons region. After heat treatment, the voids or free carbons region changed to have a clod like feature with average sizes of 50 to 100 nm (Fig. 6(b)). They were distributed not randomly but, like roughly, lines, although the intervals of them were increased after heat treatment. Moreover, the ZrC grains were slightly grown in this area with heat treatment.

A TEM image of the clods of the free carbons or voids after heat treatment is shown in Fig. 7. The free carbons region or voids show a brighter contrast than the surrounding ZrC grains. An aggregate feature of ribbons with widths of 5 to 10 nm was observed in each clod. The c-plane contrast of carbons was found in each ribbon along the elongated directions. Each ribbon would be free carbons. The free carbons region would have a sheet like shape with the c axis roughly perpendicular to the thickness direction of the sheet before heat treatment, and

would be swept out to ZrC grain boundaries due to the growth of the ZrC grains, keeping the sheet like feature, though they became crumpled.

The turbostratic carbons were observed on the IPyC/ZrC boundary similar to those observed before heat treatment.

3.3.3 Near Stoichiometric ZrC Layers (batches E, F, G and H)[17)]

3.3.3.1 Fracture Surfaces of Various Near Stoichiometric ZrC Layers

Fracture surfaces of the ZrC layers of batches E, F, G and H, with C/Zr ratios of nearly 1.0 (as shown in Table 2), were observed by SEM. Before heat treatment, the fracture surfaces of the ZrC layers seemed to show columnar characteristics, but the outlines of the crystal grains were not clearly identified in all batches, as shown in Figs. 8(a)-(d). After heat treatment, the outlines of the ZrC crystal grains were clearly identified only in batches F and H, as shown in Fig.s 8(e)-(h)[17)]. This result shows that remarkable crystal grain growth occurred with heat treatment only in batches F and H. It should especially be noted that remarkable growth in ZrC crystal grains occurred in batch F but not in batch G, as shown in Figs 8(f) and (g), in spite of both having the same C/Zr ratio and ZrC density, as shown in Table 2. Then TEM/STEM observations were carried out on batches F and G to investigate the cause of the difference in the microstructural change with heat treatment.

3.3.3.2 ZrC Layers in which Remarkable Crystal Growth Occurred (Batch F)

(1) Before Heat Treatment

Figure 9(a) shows a HAADF image of the ZrC layer near the surface of the layer. The electron diffraction image in this figure was taken by TEM.

ZrC grains were columnar in shape in the ZrC-coating layer near the surface of the ZrC layer; the average sizes of the ZrC grains were around 50 to 100 nm and 200 to 600 nm, oriented parallel to the circumferential and growth directions, respectively (Fig. 9(a)). The normals of the (110) plane of ZrC grains were oriented towards the growth direction, as shown in the electron diffraction image in Fig. 9(a). Only very few dark regions, corresponding to voids or free carbon regions, were distributed in the ZrC layer, as shown in Fig. 9(a).

Figure 9(b) show TEM images of the region including the IPyC/ZrC boundary. In the vicinity of the IPyC/ZrC boundary, the ZrC grains were granular (not columnar) in shape and their mean size was about 100 nm. IPyC and ZrC were bound to each other, as shown in Fig. 9(b). No peculiar structure including turbostratic carbon, as observed in the case of batch A (Fig. 5(b)), was observed in the boundary region.

(2) After Heat Treatment

The region including the IPyC/ZrC boundary was observed after heat treatment, as shown in Fig. 10. Remarkable ZrC grain growth occurred with heat treatment, except in the vicinity of the boundary. The ZrC grains were not columnar in shape and the size of the ZrC grains was about 5 μm at most. There was also a region where relatively small (maximum 1 μm) grains were distributed near the arrow in Fig. 10. The preferred orientation of the ZrC grains was not clarified from the electron diffraction. Pores were observed on the grain boundaries, as shown in Fig. 10.

A partially detached IPyC/ZrC boundary was found, as shown in Fig. 10. No peculiar structure was observed in the boundary region. The ZrC grains were around 300 nm in size and rather small on the IPyC/ZrC boundary, as shown in Fig. 10.

3.3.3.3 ZrC Layers in which Remarkable Crystal Growth did not Occur (Batch G)

(1) Before Heat Treatment

Figure 11 shows a HAADF image of the ZrC layer near the surface of the layer. The electron diffraction image in Fig. 11 was taken by TEM. The normals of the (200) plane of ZrC grains were diffusely oriented towards the growth direction, as shown in the electron diffraction image in Fig. 11. ZrC grains were columnar in shape in the ZrC-coating layer near the surface of the ZrC layer; the average sizes of the ZrC grains appeared to be around 100 nm and 250 to 300 nm, oriented parallel to the circumferential and growth directions, respectively, as shown in Fig. 11. The dark regions, corresponding to voids or free carbon regions, were distributed in lines roughly perpendicular to the growth direction.

(2) After Heat Treatment

Figure 12 shows a HAADF image of the ZrC layer near the surface of the layer. ZrC grain growth occurred with heat treatment. Most of the ZrC grains were not columnar in shape and the size of the grains was about 1 μm at most, as shown in Fig. 12.

The preferred orientation of the ZrC grains was not clarified from the electron diffraction. Pores were observed on the grain boundaries, as shown in Fig. 12. A relatively large pore was found to include carbons, as shown with the arrow in Fig. 12.

3.3.3.4 Difference in Microstructures of ZrC Layers of Batches F and G[17)]

TEM/STEM observation of the specimens before heat treatment clarified that many more free carbons or voids were distributed in the ZrC layer in batch G than in batch F, as shown in Fig. 13. It would be reasonable to assume that the free carbons or voids hindered ZrC crystal growth with heat treatment in batch G.

ZrC layers with a smaller grain size may be inferior to those with a larger grain size in their FP retention performance. In addition, ZrC layers in G batch would not be mechanically stronger than that in batch F in spite of the smaller grain size than that in batch F, because the grain growth with heat treatment was hindered by voids or free carbon, which is much weaker than the ZrC matrix.

In addition, the type of crystallographic orientation of the ZrC grains were different from in these two batches, as shown in electron diffractions in Figs. 13(a) and (b).

3.3.4 PAS Measurements of Various ZrC Layers[17)]

There is a possibility that many more free carbons or voids are distributed in the ZrC layer of batch X than in that of batch Y, in spite of both having the same C/Zr ratio and ZrC density, as the ZrC phase has a large composition range in carbon-poor regions. (Batches X and Y are not specific batches) That is to say, there is a possibility that,

- ✓ the ratios of free carbon to the total carbon differ in the two ZrC layers,
- ✓ and/or, vacancy densities in ZrC phase differ in two ZrC layers,

in spite of both having the same C/Zr ratio and ZrC density. We, therefore, carried out PAS measurement of various ZrC layers, including near stoichiometric ZrC layers of the above mentioned four batches, because PAS characteristics is very sensitive to vacancy density.

Figure 14 shows the S and W parameters obtained through DBAR measurements of the ZrC layers in various batches before heat treatment, as listed in Table 2. There were two clearly separated groups on the S-W plane. One included batches A and D with a high C/Zr ratio (1.35), exhibiting higher S and lower W parameters. The other included batches E, F, G and H with C/Zr of around 1.0, exhibiting lower S and higher W parameters. In the latter group, moreover, batches F and H, in which remarkable ZrC grain growth was observed by SEM as shown in Figs 8(f) and (h), gave rise to even lower S and higher W parameters. It is interesting to note that the S and W parameters of the ZrC layers fabricated in batches F and G were significantly different to each other even though the C/Zr ratios and the material densities for these specimens were nearly the same as shown in Table 2.

Although the C/Zr ratio and density of the ZrC layers of batches E, F, G and H were similar, as shown in Table 2, remarkable differences were observed in the microstructures of these layers after heat treatment, as shown in Fig. 8(e)-(h). It should be noted that batches F

and G were fabricated under similar conditions and that the C/Zr ratio and density of the ZrC layers were estimated to be same.

The FP retention performance and mechanical properties of the ZrC layers appears to depend strongly on microstructure after heat treatment, including ZrC grain size. Thus, the quality of the ZrC layers of the coated fuel particles must be controlled to give the microstructure of the ZrC layer desirable characteristics after the fuel compact sintering process. This makes it clear that measurements of the C/Zr ratio and ZrC density are not sufficient for quality control of the ZrC layers.

On the other hand, there is a clear correlation between the microstructure of ZrC layers after heat treatment and the S and W parameters of the ZrC layers before heat treatment (Fig. 14). It should especially be noted that differences between batches F and G, which could not be detected by estimating the C/Zr ratio and ZrC density, could be detected with PAS. In addition, specimen preparation for PAS is much easier than that for TEM/STEM observation. Moreover, PAS is much more suitable for quantitative evaluation than microstructural observation. Thus, PAS might be suitable as a method of quality control for ZrC-coated fuel particles.

4. Summary

We had carried out the R&Ds of fabrication technology of ZrC coated particles to improve performance of VHTR, at JAEA from 2004 to 2008.

(1) At the beginning of the R&Ds, ZrC coating temperatures were controlled by the feed-back control of the power of high-frequency coil. Then the coating temperature was oscillated. The oscillated deposition temperature resulted in non-uniform distribution of the free carbon region in ZrC layer.

(2) After the stabilization of the coating temperatures, the ZrC deposition tests were carried out at various coating temperatures to find the coating temperature for less excess carbon. The microstructures of the uniform ZrC layers with much excess carbon, fabricated in this step, were observed to obtain the knowledge on the microstructure of excess carbons in ZrC layers and the effects of heat treatment on the excess carbons.
   - The free carbon regions, with laminar features, were distributed in the ZrC layer uniformly and quite densely.
   - After heat treatment, the free carbons region changed to have a clod like feature.

(3) Coating continuously near stoichiometric ZrC and OPyC layers in the batch scale of 100 g was succeeded, after the material gas flow rates were optimized. The coated particles with nearly stoichiometric ZrC and OPyC layers are a goal in this R&Ds.

- It was, however, clarified that remarkable growth in ZrC crystal grains occurred in one batch (batch F) but not in another batch (batch G) by heat treatment, in spite of both having the same C/Zr ratio and ZrC density by SEM observation.
- TEM/STEM observation of the specimens before heat treatment clarified that many more free carbons or voids, which would hinder ZrC crystal grain growth with heat treatment, were distributed in the ZrC layer in batch G than in batch F.

(4) PAS measurement of various ZrC layers, including batches F and G, was carried out because PAS characteristics are very sensitive to vacancy density. There is a possibility that vacancy densities in ZrC phase differ in the ZrC layers of the above mentioned batches F and G, in spite of both having the same C/Zr ratio and ZrC density.

- There was a clear correlation between the microstructure of ZrC layers after heat treatment and the S and W parameters of ZrC layers before heat treatment.
- Then, PAS might be suitable as a method of quality control for ZrC-coated fuel particles, as preparing specimens for PAS is much easier than for TEM/STEM observation.

Acknowledgement

This paper includes reprinting from Journal of the American Ceramics Society and Journal of Nuclear Materials. The present study includes the result of “Development for Advanced High Temperature Gas Cooled Reactor Fuel and Graphite Components” entrusted to the Japan Atomic Energy Agency (JAEA) by the Ministry of Education, Culture, Sports, Science and Technology of Japan (MEXT).

References

1) K. Fukuda, T. Ogawa, K. Hayashi, S. Shiozawa, H. Tsuruta, I. Tanaka, N. Suzuki, S. Yoshimuta, and M. Kaneko, “Research and Development of HTTR Coated Particle Fuel,” J. Nucl. Sci. Technol., 28, p. 570, (1991).
2) U.S.DOE Nuclear Energy Research Advisory Committee and the Generation IV International Forum, 03-GA500034-08, (2004).
3) T. Ogawa, K. Ikawa, K. Iwamoto, “Chemical vapor deposition of ZrC within a spouted bed by bromide process”, J. Nucl. Mater. 97, p. 104 (1981).
4) T. Ogawa, K. Fukuda, S. Kashimura, T. Tobita, F. Kobayashi, S. Kado, H. Miyanishi, I. Talahashi and T. Kikuchi, “Performance of ZrC-Coated Particle Fuel in Irradiation and Postirradiation Heating Tests”, J. Am. Ceram. Soc. 75, p. 2985, (1992).

5) T. Ogawa and K. Ikawa, “Reaction of Pd with SiC and ZrC”, High Temp. Sci., 22 p. 179, (1986).
6) A. Yasuda, S. Ueta, J. Aihara, H. Takeuchi and K. Sawa, “Development of Production Technology of ZrC-coated Particle (No. 1)”, JAEA-Technology 2008-073, Japan Atomic Energy Agency (JAEA), (2008). (in Japanese)
7) A. Yasuda, S. Ueta, J. Aihara, H. Takeuchi and K. Sawa, “Development of Production Technology of ZrC-coated Particle (No. 2)”, JAEA-Technology 2008-083, Japan Atomic Energy Agency (JAEA), (2008). (in Japanese)
8) S. Ueta, J. Aihara, A. Yasuda, H. Ishibashi, Y. Mozumi, K. Sawa and K. Minato, “Development on fabrication techniques for the ZrC-coated fuel particle as an advanced high temperature gas cooled reactor fuel”, Hyomen, 46, p. 222, (2008). (in Japanese)
9) S. Ueta, J. Aihara, A. Yasuda, H. Ishibashi, T. Takayama and K. Sawa, “Fablication of uniform ZrC coating layer for the coated fuel particle of the very high temperature reactor”, J. Nucl. Mater., 376 p. 146, (2008).
10) Report of “Research and development for advanced high temperature gas cooled reactor and graphite components” in fiscal year 2008, entrusted to the Japan Atomic Energy Research Institute by the Ministry of Education, Culture, Sports, Science and Technology of Japan (MEXT). (in Japanese)
11) G. Vasudevamurthy, Y. Katoh, J. Aihara, K. Sawa and L. L. Snead, “Microstructure of Irradiated ZrC TRISO Coatings”, American Nuclear Society: 2010 Winter Meeting and Nuclear Technology Expo, 7-11 Nov. 2010, Nevada, USA.
12) S. Ueta, J. Aihara, K. Sawa, A. Yasuda, M. Honda and N. Furihata, “Development of high temperature gas-cooled reactor (HTGR) fuel in Japan”, Progress in Nucl. Ener. 53, p. 788, (2011).
13) G. Vasudemurthy, Y. Katoh, J. D. Hunn and L. L. Snead, “Pre- and Post-Irradiation Characterization and Properties Measurements of ZrC-coated Surrogate TRISO Particles”, ORNL/TM-2010/223 (2010).
14) J. Aihara, S. Ueta, T. Shibata and K. Sawa, “Code-B-1 for Stress/Strain Calculation for TRISO Fuel Particle (Contract Research)”, JAEA-Data/Code 2011-016 (2011).
15) J. Aihara, S. Ueta, A. Yasuda, H. Ishibashi, Y. Mozumi, K. Sawa and Y. Motohashi, “TEM/STEM Observation of ZrC Coating Layer for Advanced High-Temperature Gas-Cooled Reactor Fuel, Part II”, J. Am. Ceram. Soc. 92, p. 197, (2009).
16) J. Aihara, S. Ueta, A. Yasuda, H. Takeuchi, Y. Mozumi, K. Sawa and Y. Motohashi, “Effect of Heat Treatment on TEM Microstructures of Zirconium Carbide Layer in Fuel Particle for Advanced High Temperature Gas Cooled Reactor”, Mater. Trans., 50, p. 2631, (2009).
17) J. Aihara, M. Maekawa, S. Ueta, A. Kawasuso and K. Sawa, “Microstructures and Positron Annihilation Spectroscopy of Nearly Stoichiometric ZrC Coating Layers for

Advanced High Temperature Gas-Cooled Reactor Fuel", J. Am. Ceram. Soc., 94, p. 4516, (2011).

18) J. Aihara, S. Ueta, A. Yasuda, H. Ishibashi, T. Takayama, K. Sawa and Y. Motohashi, "TEM/STEM Observation of ZrC-Coating Layer for Advanced High-Temperature Gas-Cooled Reactor Fuel", J. Am. Ceram. Soc., 90, p. 3968, (2007).

19) K. Minato and T. Ogawa, "Research and Development of ZrC-Coated Particle Fuel", Proc. GLOBAL 2003, (New Orleans, LA, USA, 2003) p. 1068, (2003).

20) T. Ogawa, K. Ikawa and K. Iwamoto, "Microhardness and Microstructure of Chemically Vapor Deposited ZrC-C Alloy", J. Nucl. Mater., 62, p.322, (1976).

21) M. Maekawa and A. Kawasuso, "Construction of a positron microbeam in JAEA", Appl. Surf. Sci. 255, p.39, (2008).

22) M. Maekawa, A. Kawasuso, T. Hirade and Y. Miwa, "Application of positron microprobe for nuclear materials", Mater. Sci. Forum, 607, p. 266, (2009).

23) M. Maekawa, A. Kawasuso, T. Hirade and Y. Miwa, "Development and application of positron microprobe", Trans. Mater. Res. Soc. Jap. 33, p. 334, (2008).

24) A. T. Matveev, D. Golberg, V. P. Novikov, L. L. Klimkovich and Y. Bando, "Synthesis of Carbon Nanotubes below Room Temperature", Carbon, 39 p. 155, (2001).

25) D. Helary, O. Dugne and X. Bourrat, "Advanced Characterization Techniques for SiC and PyC Coatings on High-Temperature Reactor Fuel Particles", J. Nucl. Mater. 373, p. 150, (2008).

26) E. Pollmann, J. Pelissier, C. S. Yust, J. L. Kaae, "Transmission Electron Microscopy of Pyrocarbon Coatings", Nucl. Technol. 35, p. 301, (1977).

Table 1 Materials and the roles of each coating layer

Coating layer	Material	Role
Buffer layer	Low density pyrolytic carbon	Plenum for gases (gaseous fission products, CO gas)
Inner pyrolytic carbon (IPyC) layer	High density pyrolytic carbon	• Retaining gases • Protest UO_2 kernel from material gas during deposition of the third layer
The third layer	Silicon carbide (SiC)	• Main structural layer • Barrier for metallic fission products
Outer pyrolytic carbon (OPyC) layer	High density pyrolytic carbon	Cushion for the third layer

Table 2 Basic data on coated particles[15-18] and summary of detailed characterization.

Batch	Nominal ZrC deposition temperature [K]	C/Zr ratio	Density of ZrC Layer [g/cm^3]	Remarkable grain growth with heat treatment	Voids or free carbons		S and W parameters	note
A	1769	1.35	6.01	no	Very dense		See Fig. 14	
D	1723	1.36	6.15	Not studied	Not studied			
E	1637	1.03	6.50	no				
F	1632	1.03	6.52	yes	Very few	See Fig. 13		With OPyC layer
G	1627	1.03	6.52	no	Denser than F			
H	1557	1.05	6.52	yes	Not studied			Almina kernel*1
I	1493–1823 (oscillated)	Not measured	Not measured	Not studied	Very dense		Not measured	

*1 For batch H, alumina kernels were used instead of zirconia kernels to reduce radioactivity after irradiation tests with nuclear reactors[17].

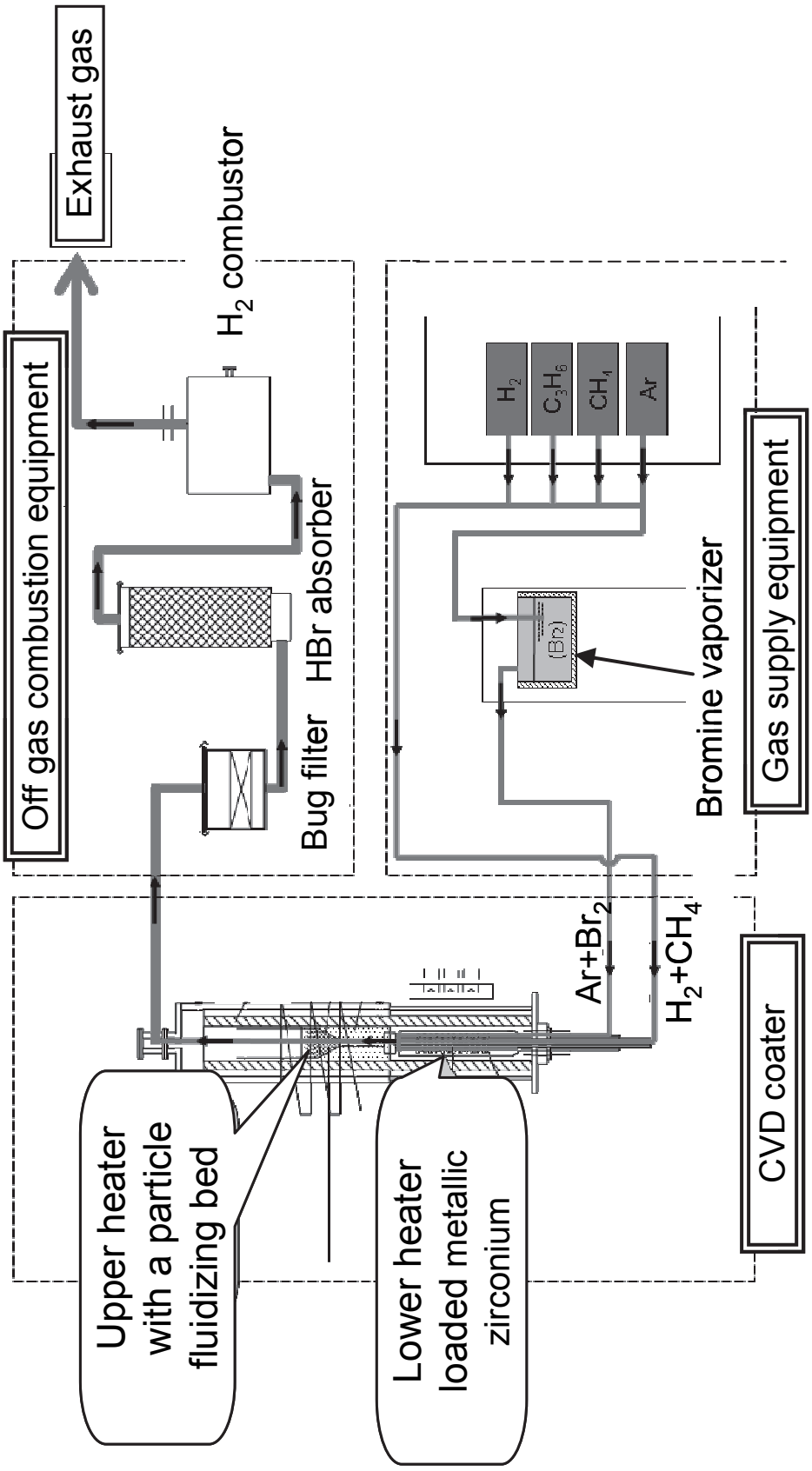

Fig. 1 Process flow diagram of ZrC coater[9].

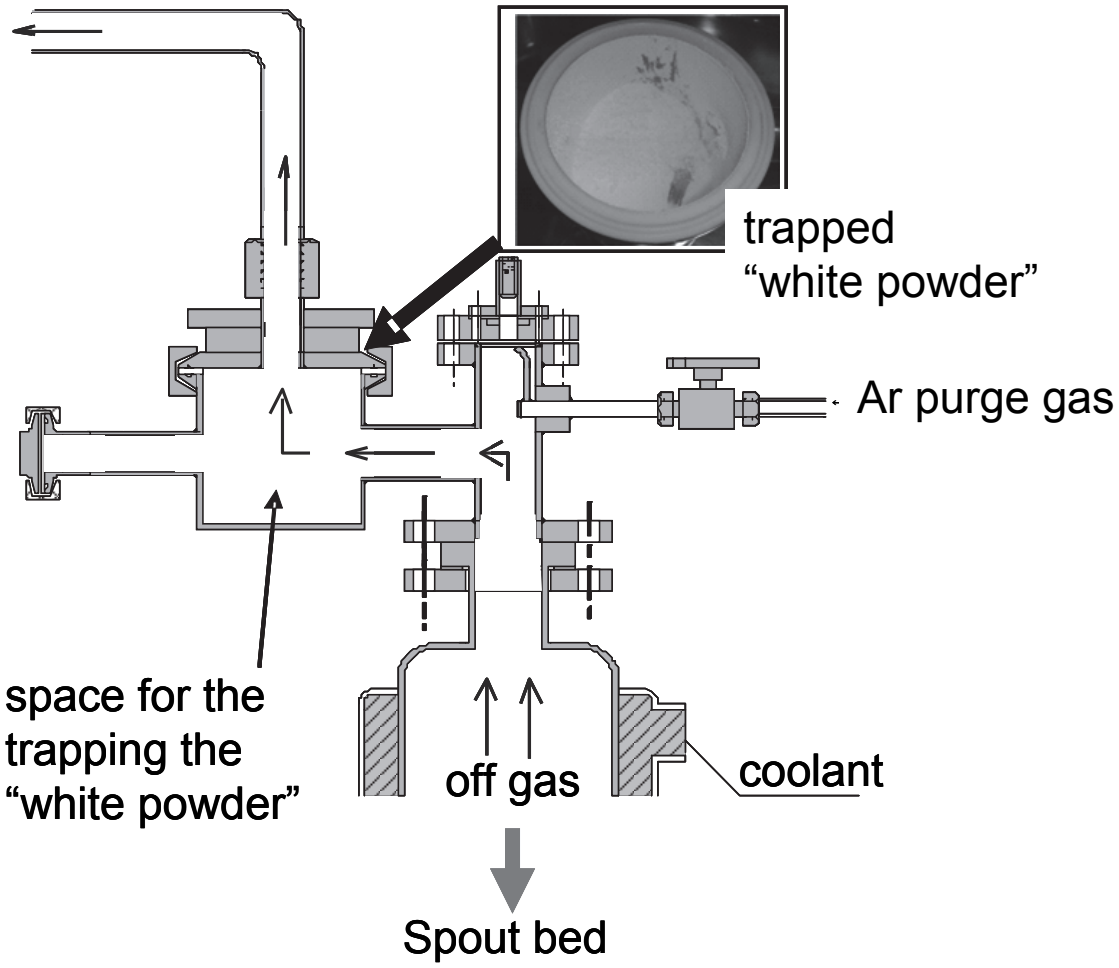

Fig. 2 Space for trapping “white powder”[6].

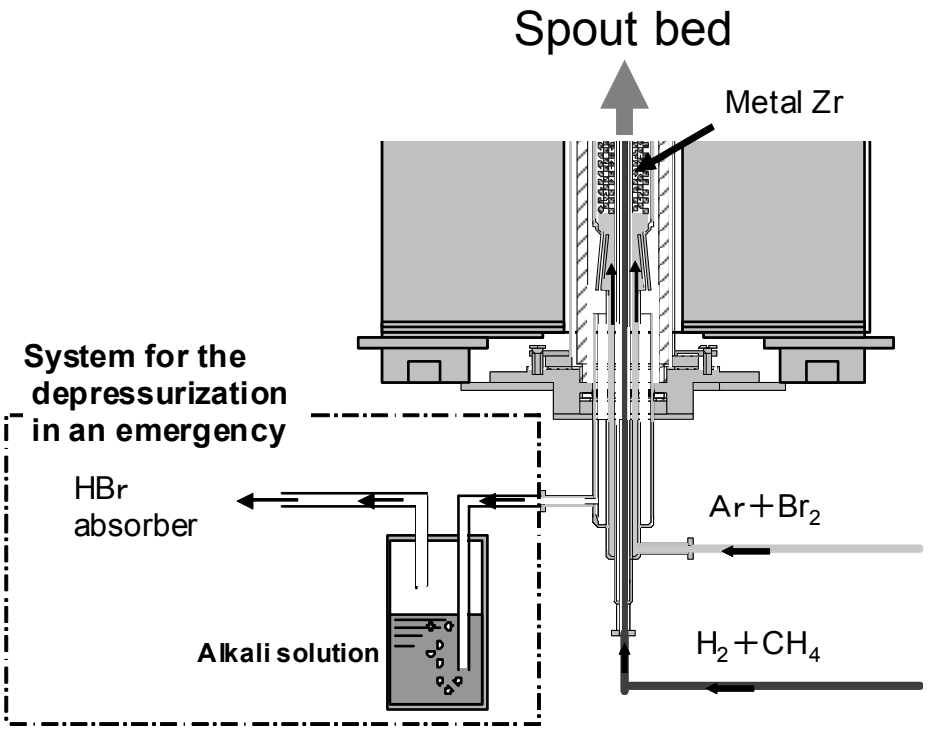

Fig. 3 System for depressurization in an emergency[6].

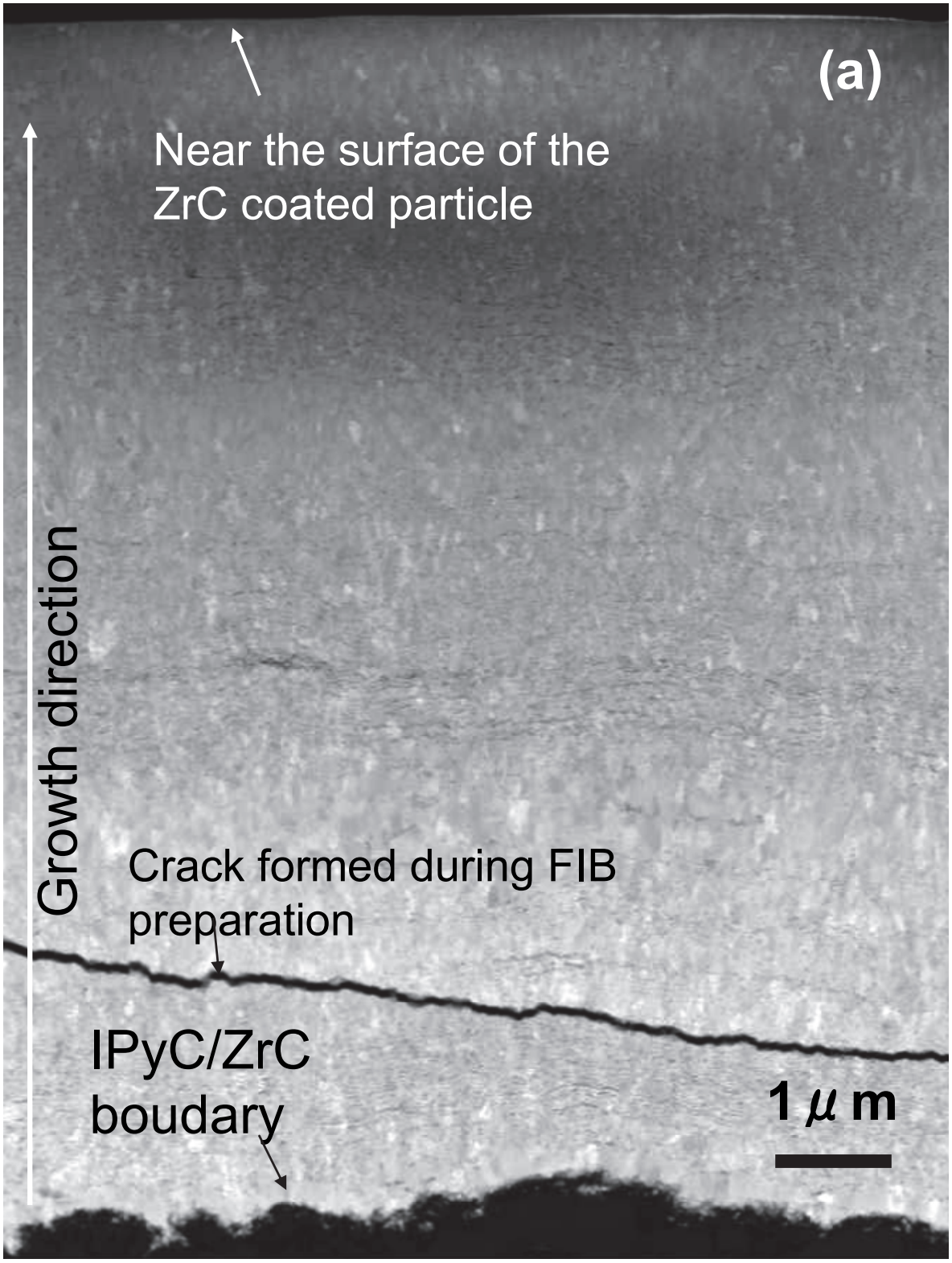

Fig. 4(1/2) TEM/STEM images of ZrC layer of batch I[18], (a) HAADF image ZrC layer.

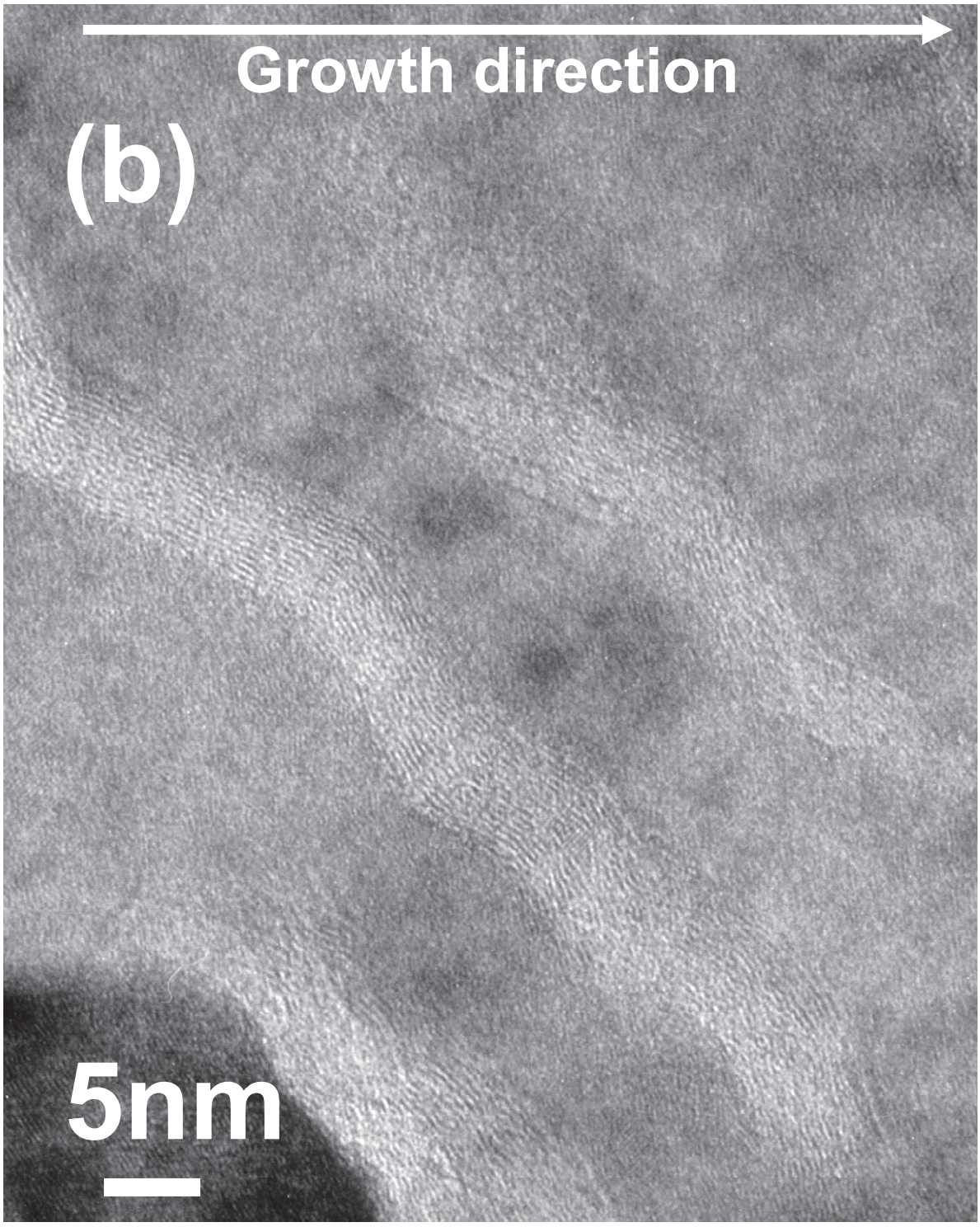

Fig. 4(2/2) TEM/STEM images of ZrC layer of batch I[18], (b) high resolution TEM image of free carbon region.

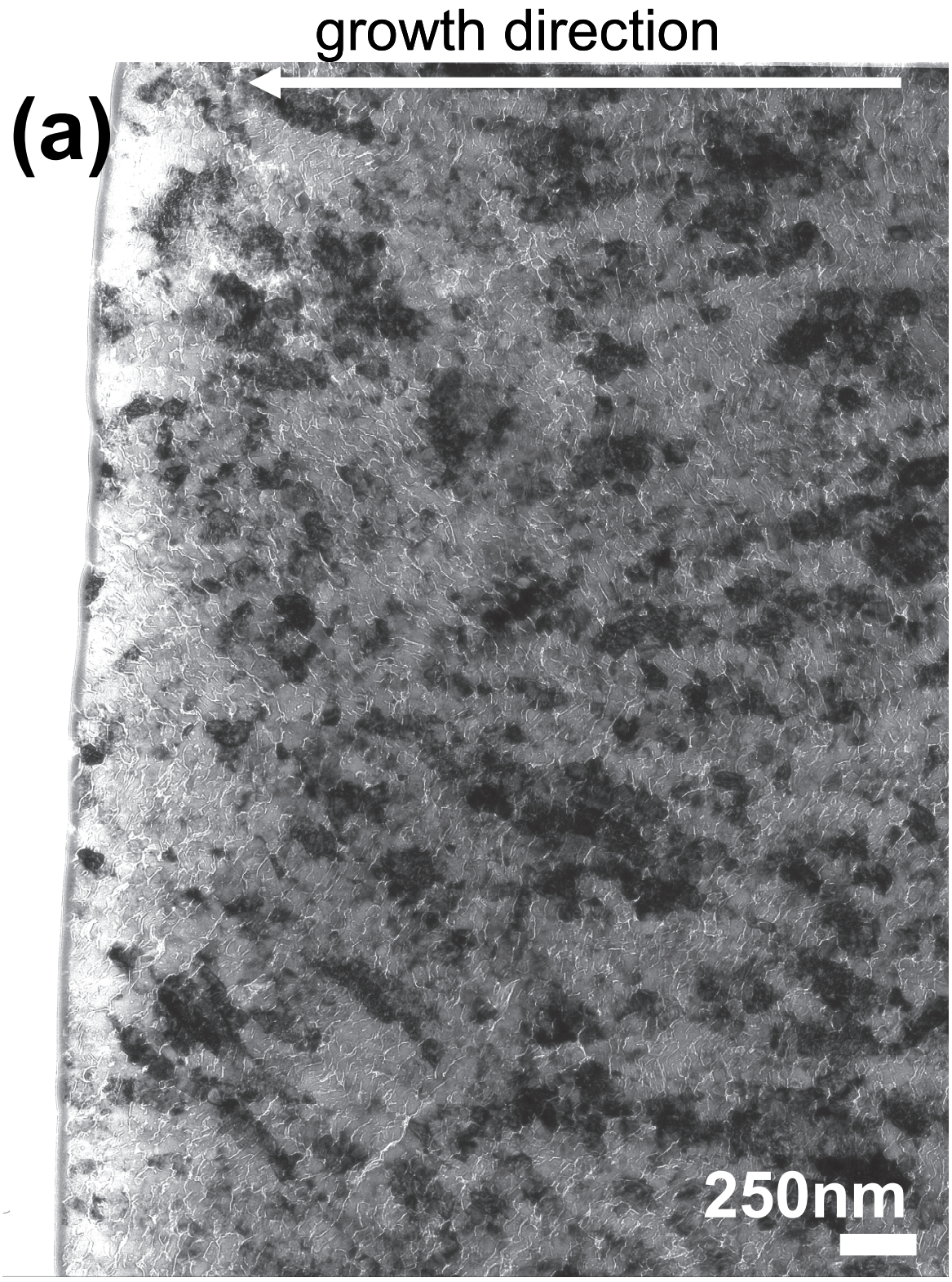

Fig. 5(1/2) TEM images of ZrC layer of batch A before heat treatment[15], (a) bright field image of ZrC layer,

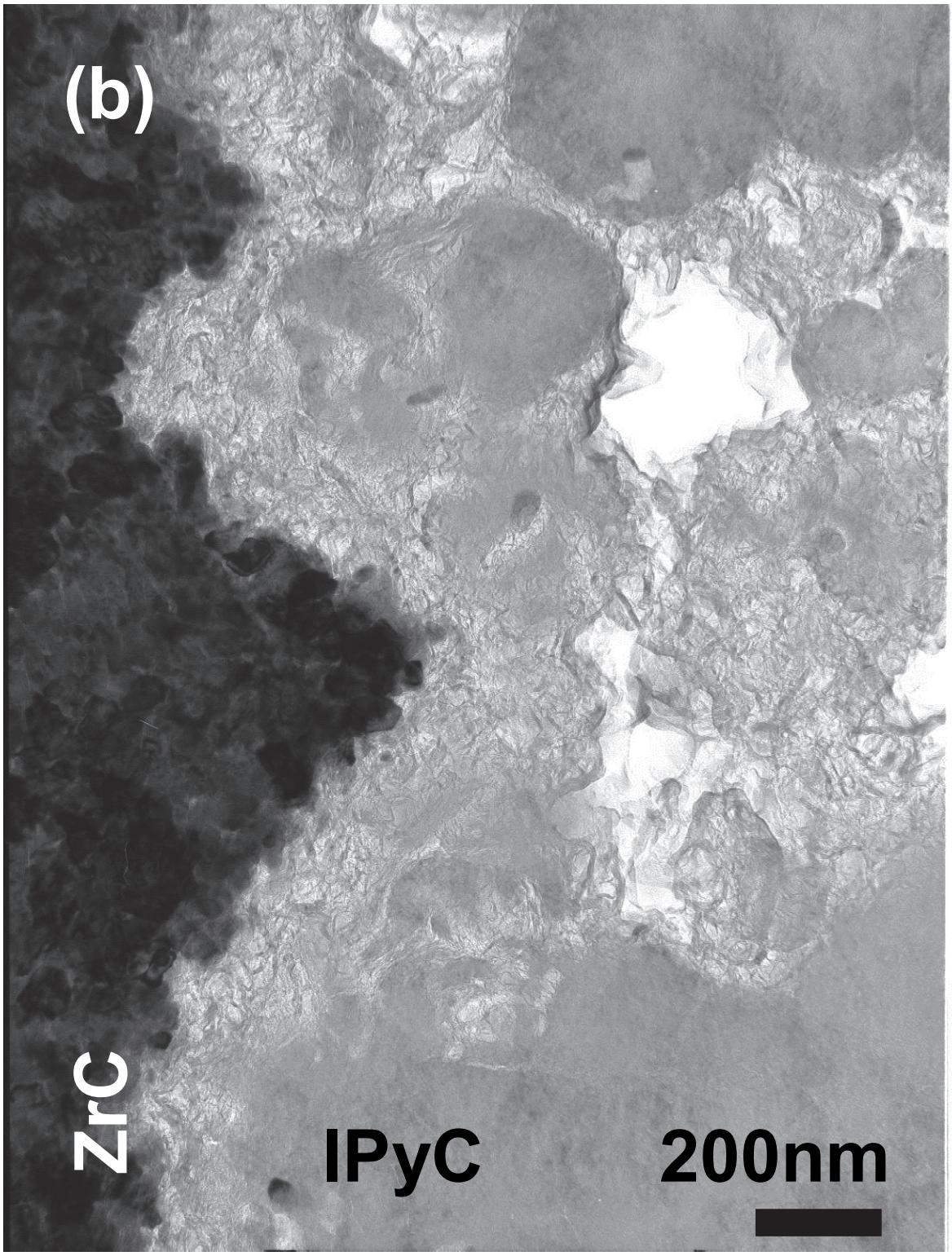

Fig. 5(2/2) TEM images of ZrC layer of batch A before heat treatment[15], (b) bright field image of IPyC/ZrC boundary region.

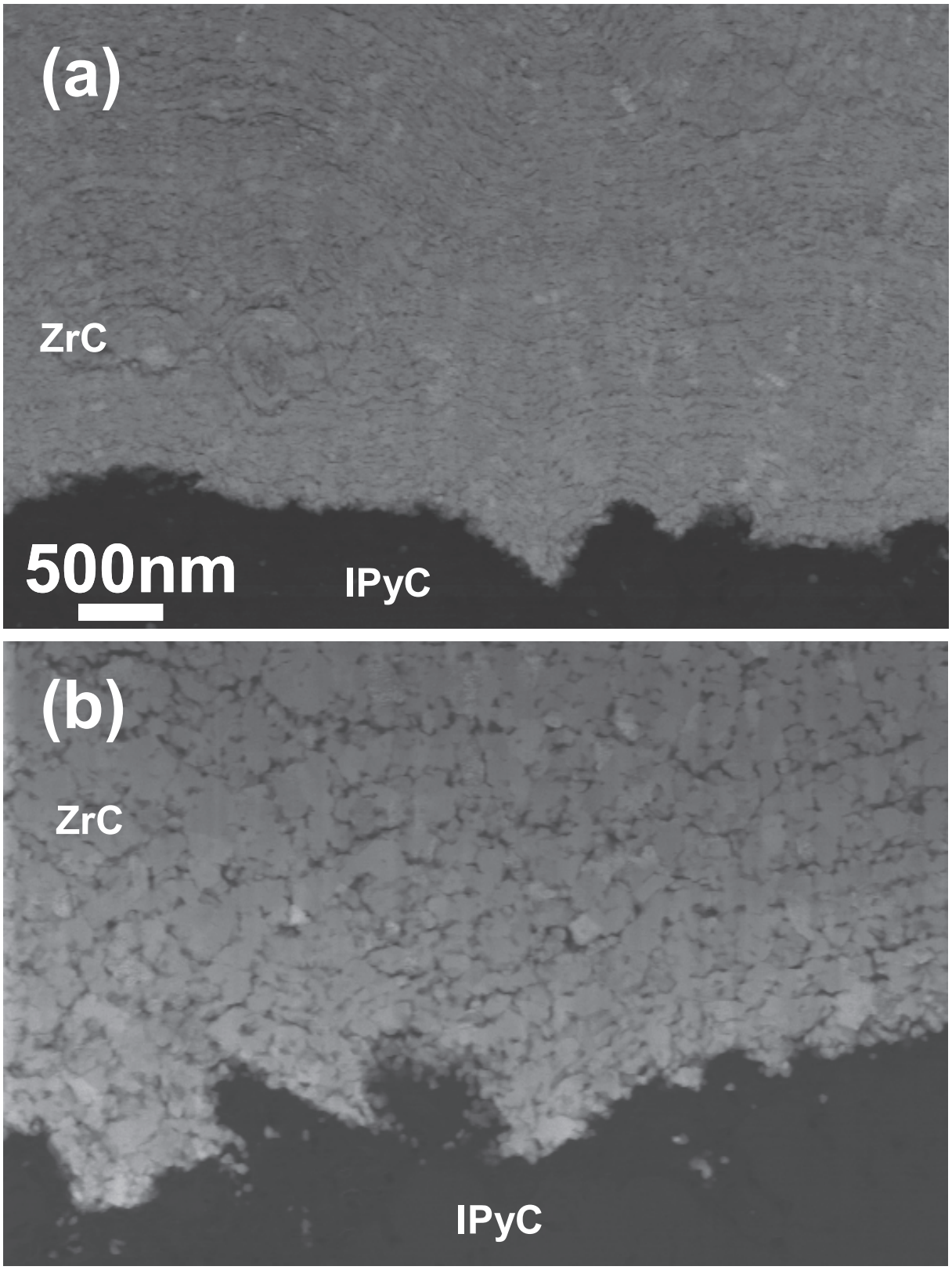

Fig. 6 HAADF images of ZrC layers of batch A[16], (a) before heat treatment, (b) after heat treatment.

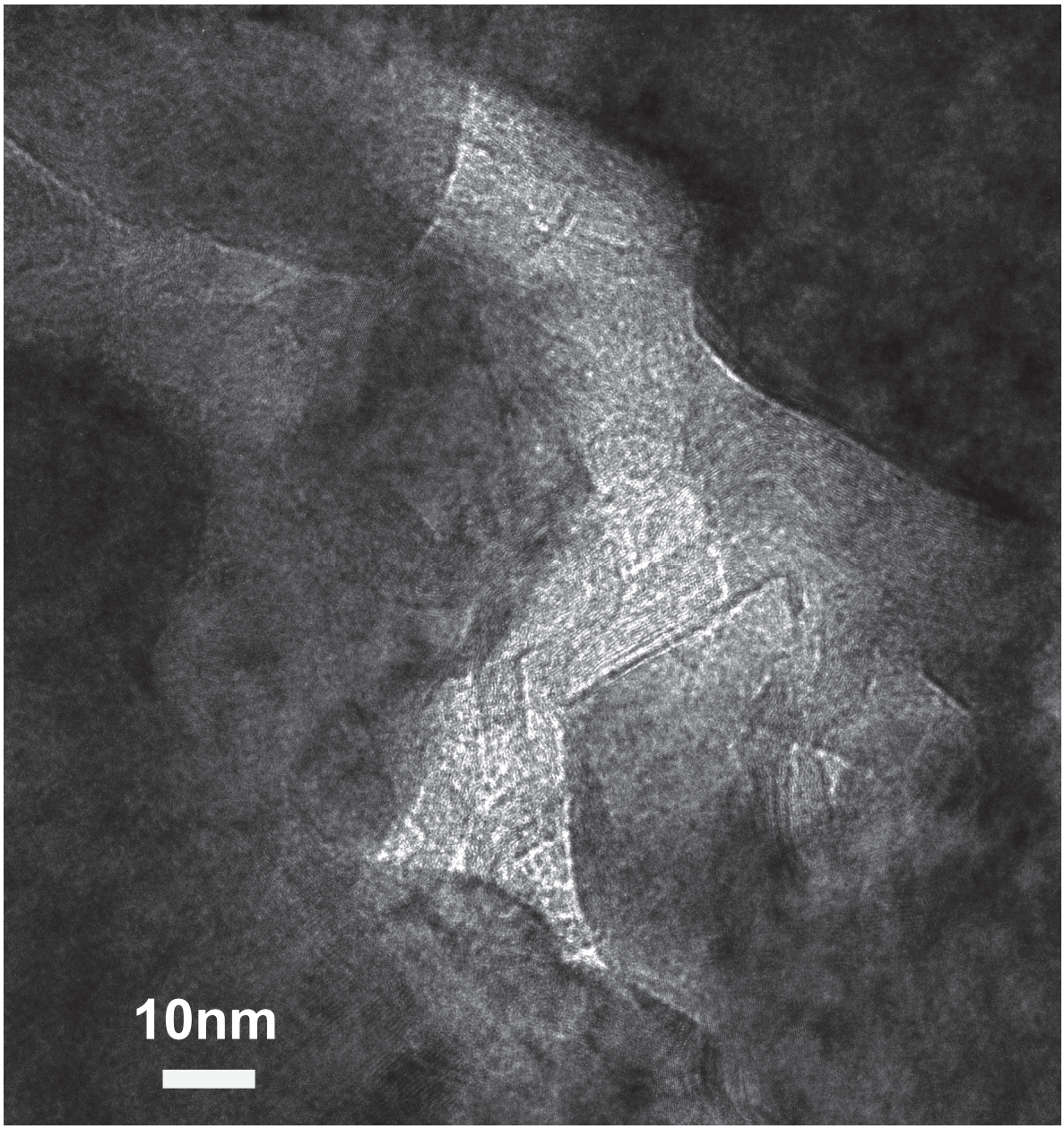

Fig. 7 TEM image of clod of free carbon in batch A after heat treatment[16].

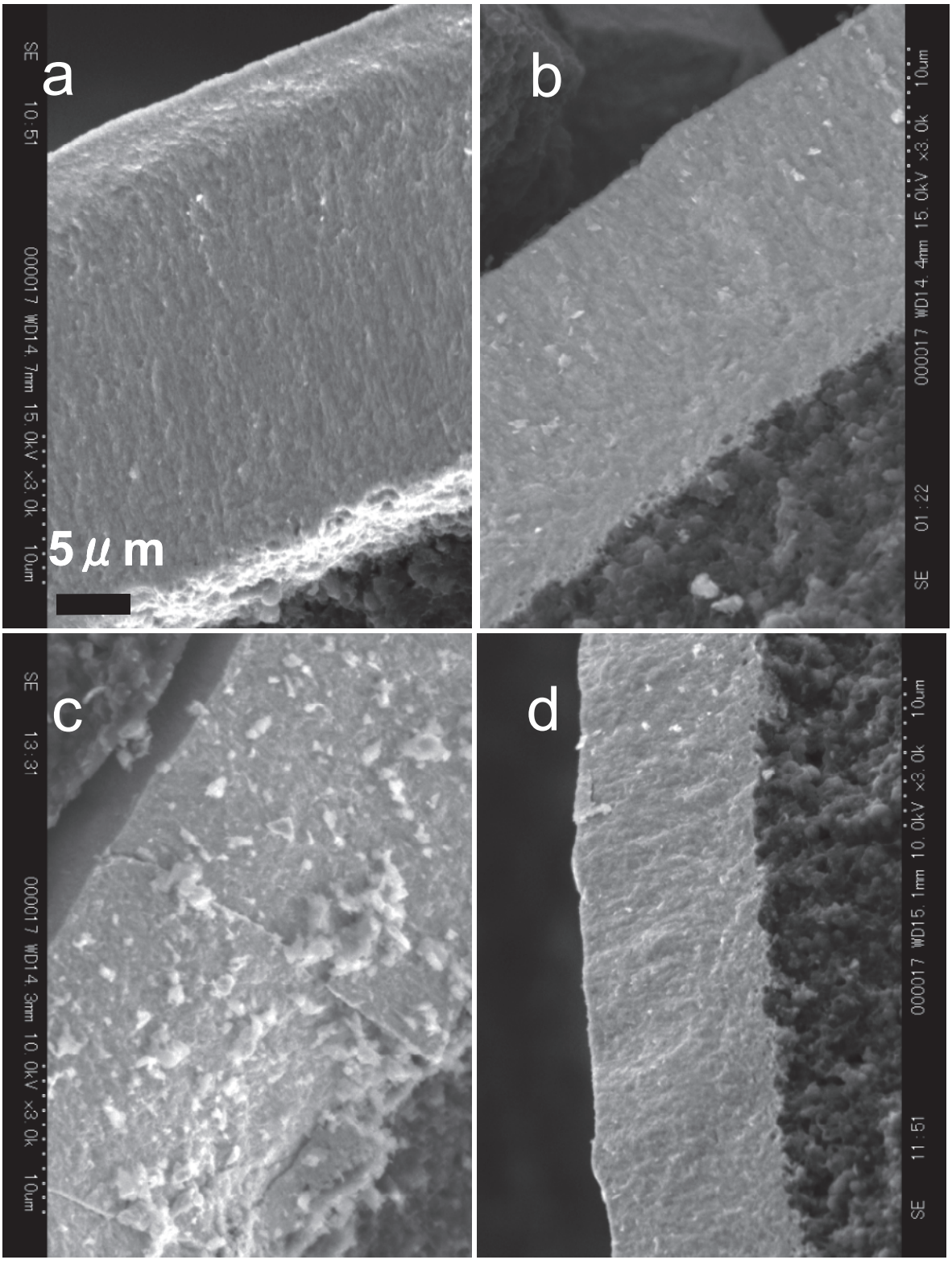

Fig. 8(1/2) SEM images of fracture surfaces of near stoichiometric ZrC layers before and after heat treatment, (a) E batch (before heat treatment), (b) F batch (before heat treatment), (c) G batch (before heat treatment), (d) H batch (before heat treatment).

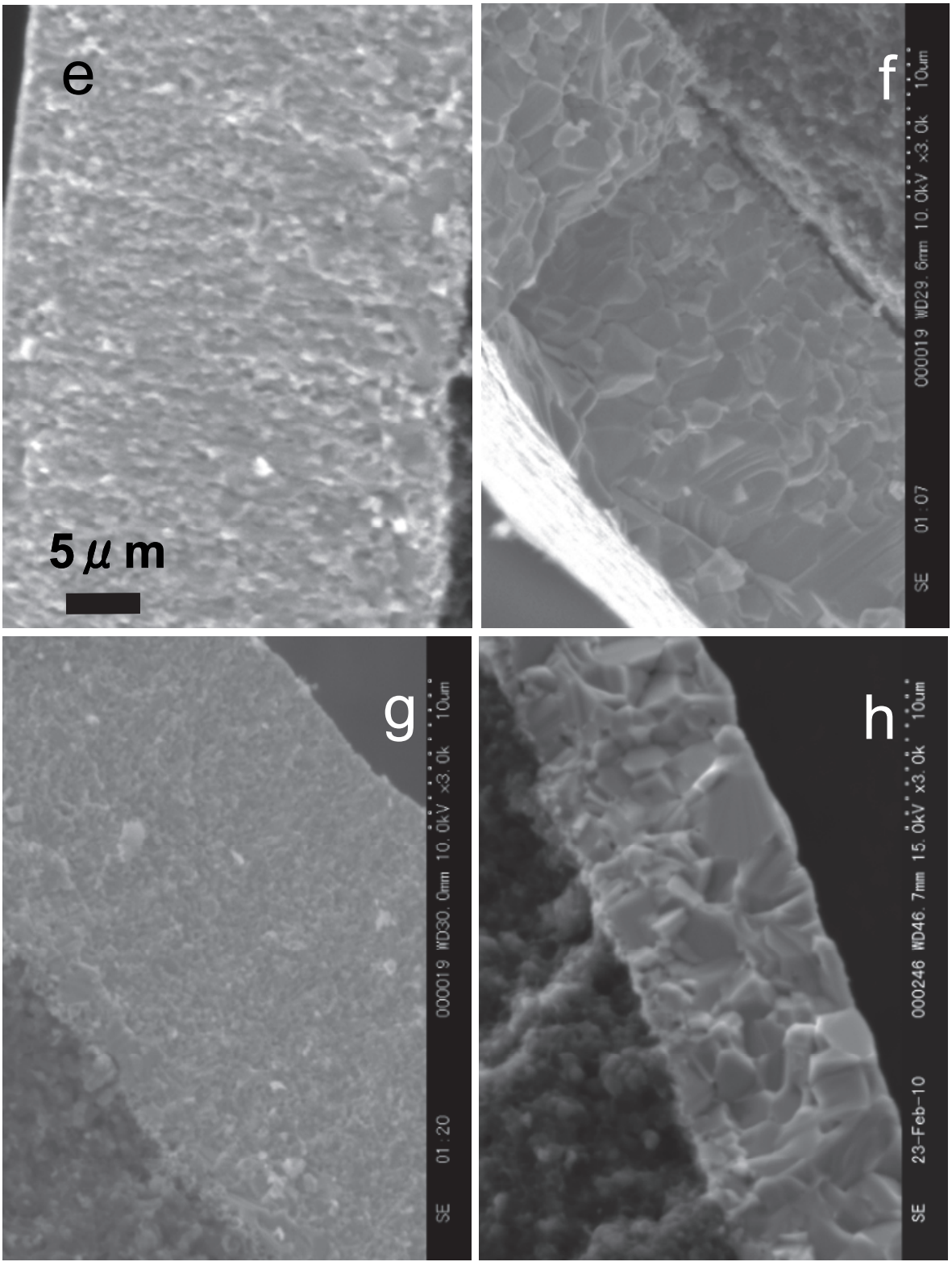

Fig. 8(2/2) SEM images of fracture surfaces of near stoichiometric ZrC layers before and after heat treatment, (e) E batch (before heat treatment)[17], (f) F batch (after heat treatment)[17], (g) G batch (after heat treatment)[17], (h) H batch (after heat treatment) [17].

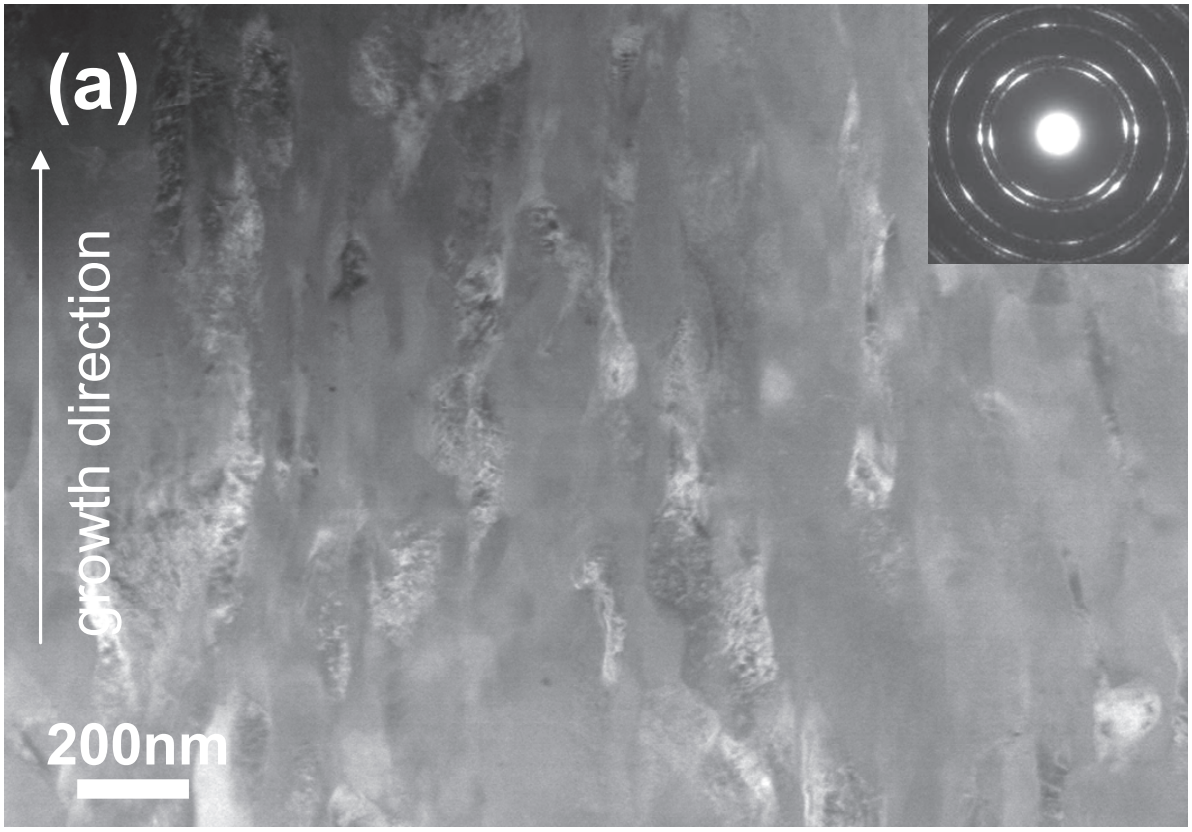

Fig. 9(1/2) TEM/STEM images of ZrC layer of batch F before heat treatment[17], (a) HAADF image of ZrC layer (electron diffraction image was taken with TEM).

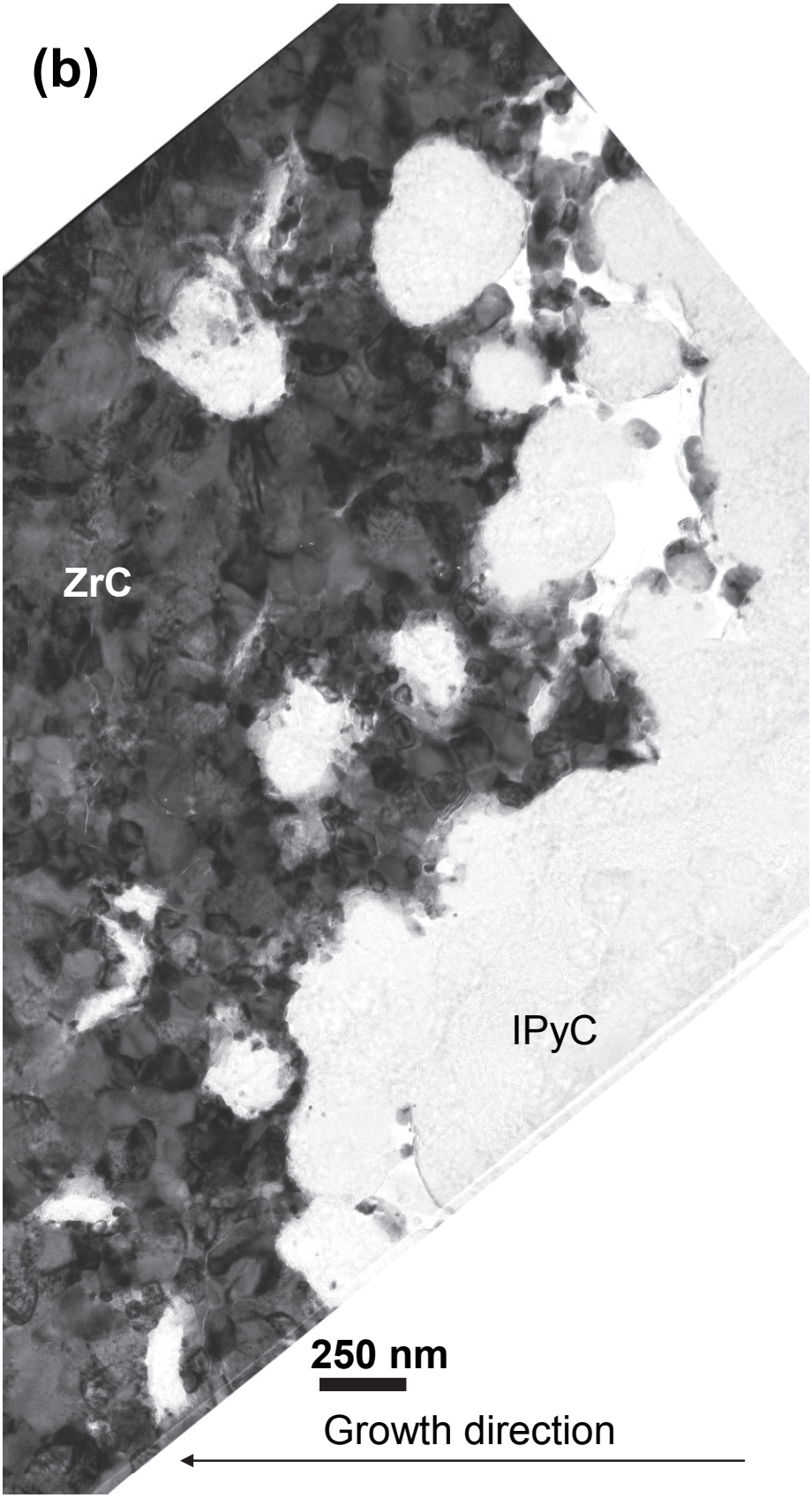

Fig. 9(2/2) TEM/STEM images of ZrC layer of batch F before heat treatment[17], (b) IPyC/ZrC boundary region.

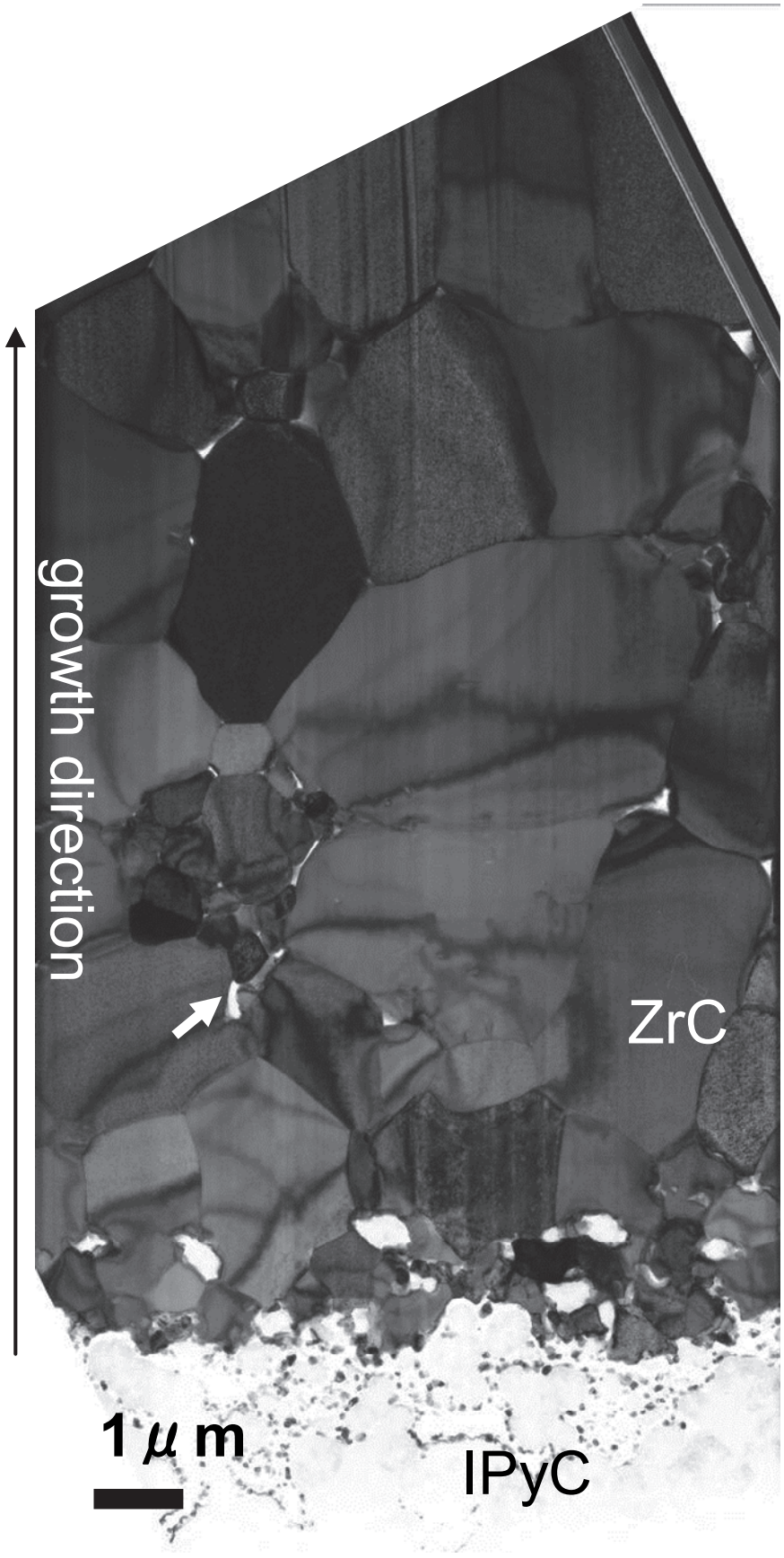

Fig. 10 TEM image of ZrC layer of batch F after heat treatment[17].

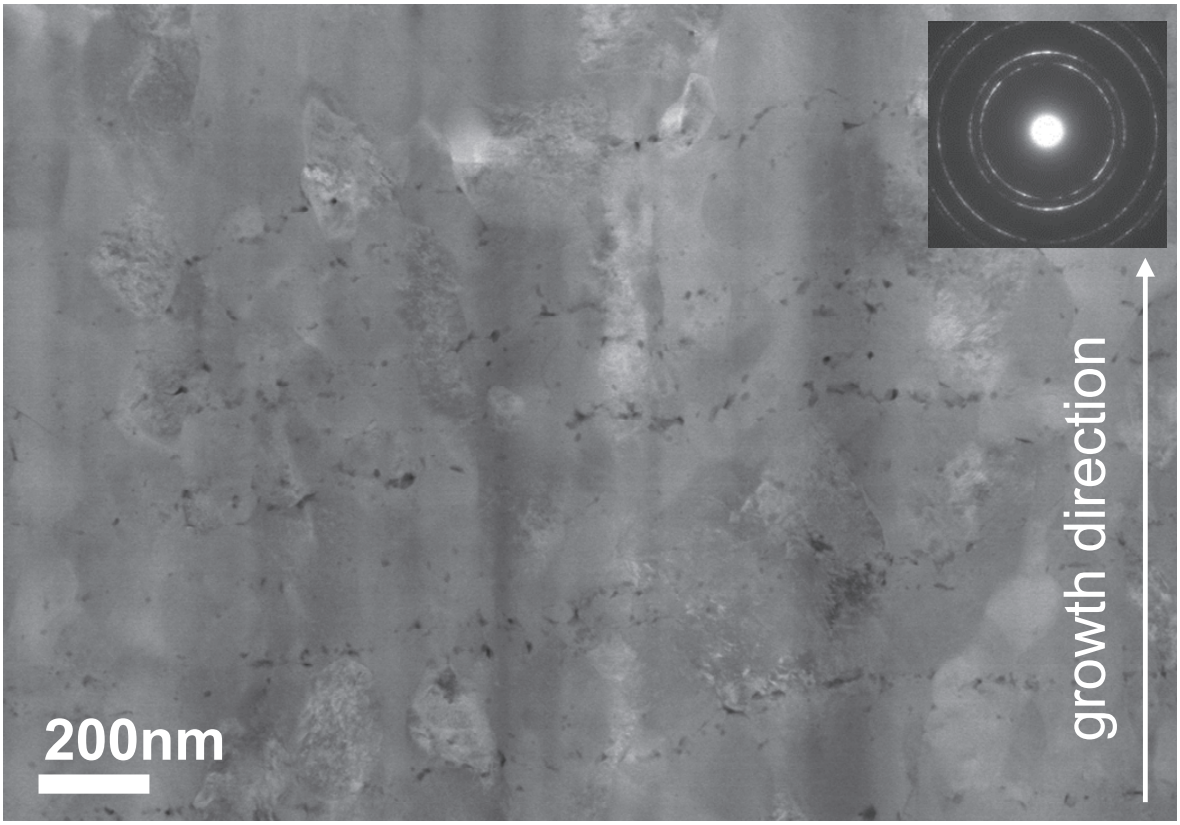

Fig. 11 HAADF image of ZrC layer of batch G before heat treatment (electron diffraction image was taken with TEM)[17].

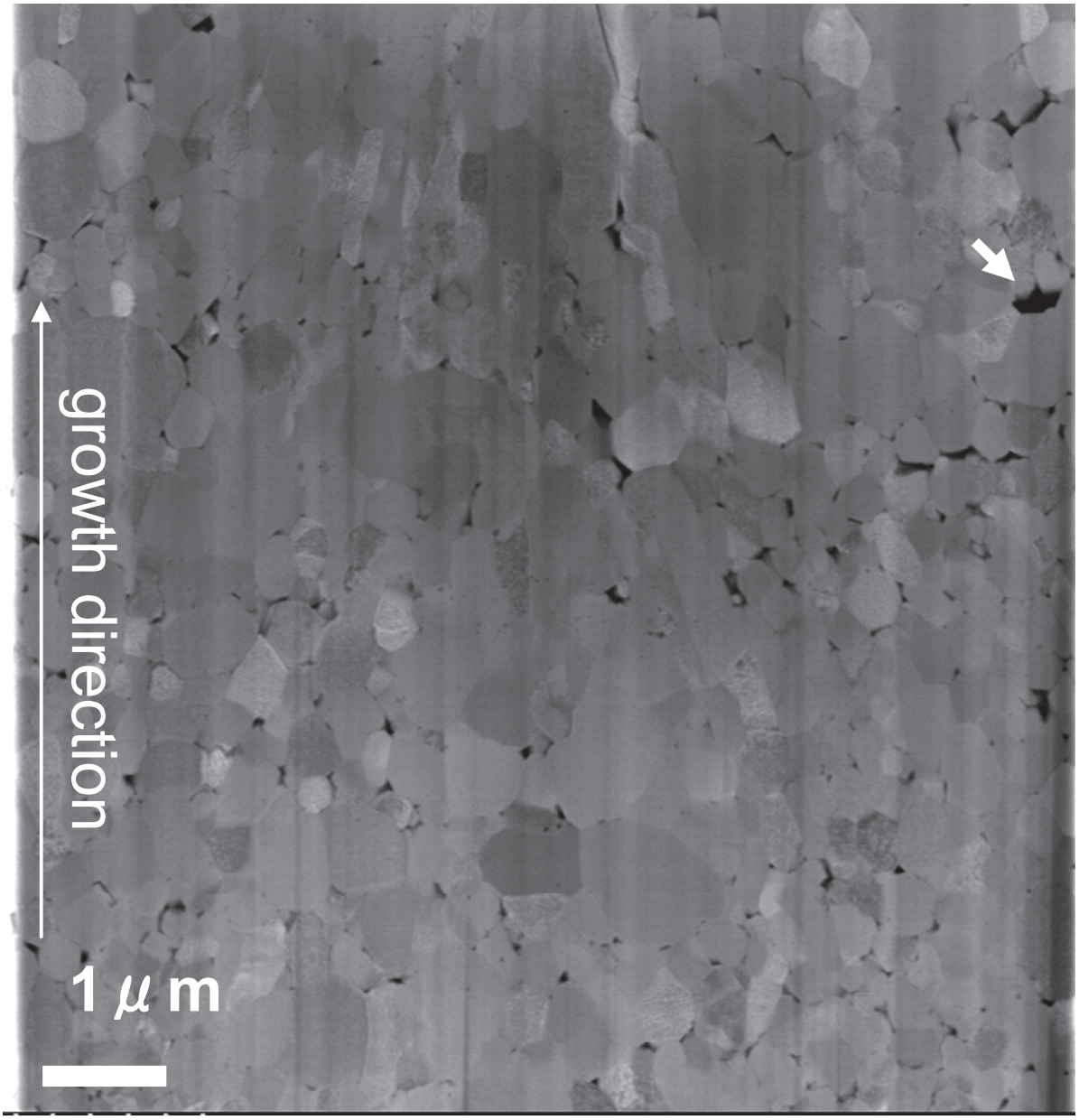

Fig. 12 HAADF image of ZrC layer of batch G after heat treatment[17].

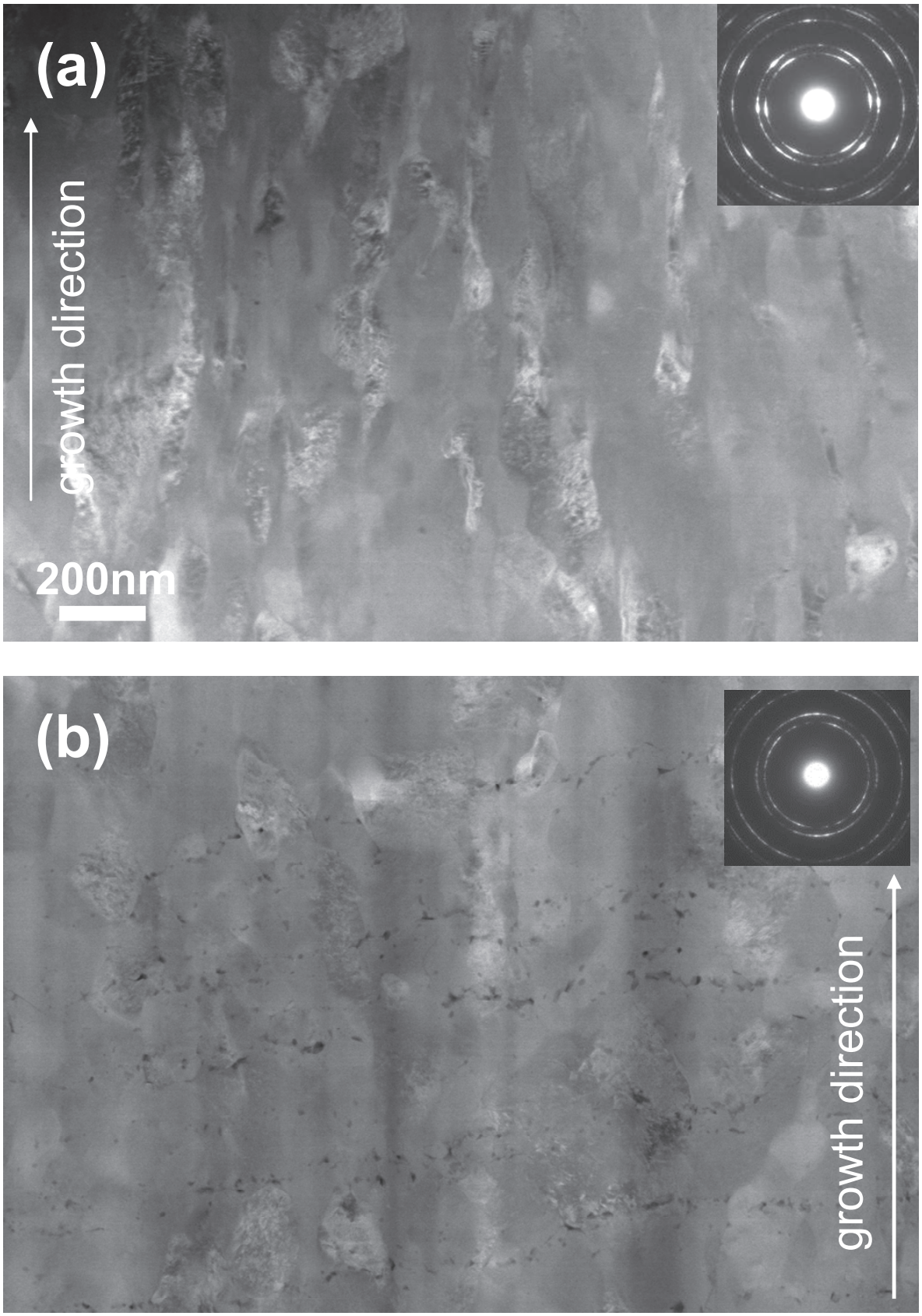

Fig. 13 HAADF images of ZrC layers before heat treatment[17], (a) batch F, (b) batch G.

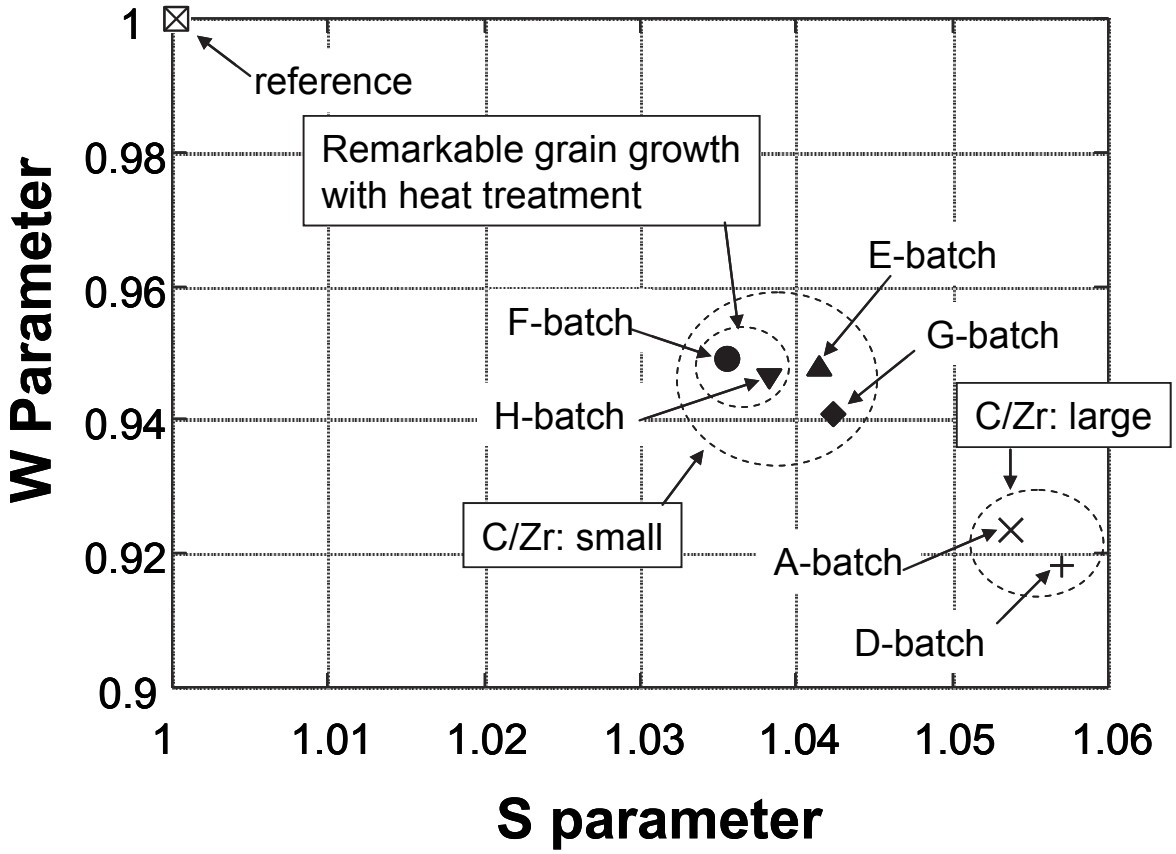

Fig. 14 S and W parameters on surface of ZrC layers of various specimens before heat treatment[17].

国際単位系（SI）

表１．SI 基本単位

基本量	SI 基本単位	
	名称	記号
長さ	メートル	m
質量	キログラム	kg
時間	秒	s
電流	アンペア	A
熱力学温度	ケルビン	K
物質量	モル	mol
光度	カンデラ	cd

表２．基本単位を用いて表されるSI組立単位の例

組立量	SI 基本単位	
	名称	記号
面積	平方メートル	m^2
体積	立法メートル	m^3
速さ，速度	メートル毎秒	m/s
加速度	メートル毎秒毎秒	m/s^2
波数	毎メートル	m^{-1}
密度，質量密度	キログラム毎立方メートル	kg/m^3
面積密度	キログラム毎平方メートル	kg/m^2
比体積	立方メートル毎キログラム	m^3/kg
電流密度	アンペア毎平方メートル	A/m^2
磁界の強さ	アンペア毎メートル	A/m
量濃度(a)，濃度	モル毎立方メートル	mol/m^3
質量濃度	キログラム毎立法メートル	kg/m^3
輝度	カンデラ毎平方メートル	cd/m^2
屈折率(b)	（数字の） 1	1
比透磁率(b)	（数字の） 1	1

(a) 量濃度（amount concentration）は臨床化学の分野では物質濃度（substance concentration）ともよばれる。
(b) これらは無次元量あるいは次元１をもつ量であるが、そのことを表す単位記号である数字の１は通常は表記しない。

表３．固有の名称と記号で表されるSI組立単位

組立量	SI 組立単位			
	名称	記号	他のSI単位による表し方	SI基本単位による表し方
平面角	ラジアン(b)	rad	1 (b)	m/m
立体角	ステラジアン(b)	sr(c)	1 (b)	m^2/m^2
周波数	ヘルツ(d)	Hz		s^{-1}
力	ニュートン	N		m kg s^{-2}
圧力，応力	パスカル	Pa	N/m^2	m^{-1} kg s^{-2}
エネルギー，仕事，熱量	ジュール	J	N m	m^2 kg s^{-2}
仕事率，工率，放射束	ワット	W	J/s	m^2 kg s^{-3}
電荷，電気量	クーロン	C		s A
電位差（電圧），起電力	ボルト	V	W/A	m^2 kg s^{-3} A^{-1}
静電容量	ファラド	F	C/V	m^{-2} kg^{-1} s^4 A^2
電気抵抗	オーム	Ω	V/A	m^2 kg s^{-3} A^{-2}
コンダクタンス	ジーメンス	S	A/V	m^{-2} kg^{-1} s^3 A^2
磁束	ウエーバ	Wb	Vs	m^2 kg s^{-2} A^{-1}
磁束密度	テスラ	T	Wb/m^2	kg s^{-2} A^{-1}
インダクタンス	ヘンリー	H	Wb/A	m^2 kg s^{-2} A^{-2}
セルシウス温度	セルシウス度(e)	℃		K
光束	ルーメン	lm	cd sr(c)	cd
照度	ルクス	lx	lm/m^2	m^{-2} cd
放射性核種の放射能(f)	ベクレル(d)	Bq		s^{-1}
吸収線量，比エネルギー分与，カーマ	グレイ	Gy	J/kg	m^2 s^{-2}
線量当量，周辺線量当量，方向性線量当量，個人線量当量	シーベルト(g)	Sv	J/kg	m^2 s^{-2}
酸素活性	カタール	kat		s^{-1} mol

(a)SI接頭語は固有の名称と記号を持つ組立単位と組み合わせても使用できる。しかし接頭語を付した単位はもはやコヒーレントではない。
(b)ラジアンとステラジアンは数字の１に対する単位の特別な名称で、量についての情報をつたえるために使われる。実際には、使用する時には記号rad及びsrが用いられるが、習慣として組立単位としての記号である数字の１は明示されない。
(c)測光学ではステラジアンという名称と記号srを単位の表し方の中に、そのまま維持している。
(d)ヘルツは周期現象についてのみ、ベクレルは放射性核種の統計的過程についてのみ使用される。
(e)セルシウス度はケルビンの特別な名称で、セルシウス温度を表すために使用される。セルシウス度とケルビンの単位の大きさは同一である。したがって、温度差や温度間隔を表す数値はどちらの単位で表しても同じである。
(f)放射性核種の放射能（activity referred to a radionuclide）は、しばしば誤った用語で"radioactivity"と記される。
(g)単位シーベルト（PV,2002,70,205）についてはCIPM勧告2（CI-2002）を参照。

表４．単位の中に固有の名称と記号を含むSI組立単位の例

組立量	SI 組立単位		
	名称	記号	SI 基本単位による表し方
粘度	パスカル秒	Pa s	m^{-1} kg s^{-1}
力のモーメント	ニュートンメートル	N m	m^2 kg s^{-2}
表面張力	ニュートン毎メートル	N/m	kg s^{-2}
角速度	ラジアン毎秒	rad/s	m m^{-1} s^{-1}=s^{-1}
角加速度	ラジアン毎秒毎秒	rad/s^2	m m^{-1} s^{-2}=s^{-2}
熱流密度，放射照度	ワット毎平方メートル	W/m^2	kg s^{-3}
熱容量，エントロピー	ジュール毎ケルビン	J/K	m^2 kg s^{-2} K^{-1}
比熱容量，比エントロピー	ジュール毎キログラム毎ケルビン	J/(kg K)	m^2 s^{-2} K^{-1}
比エネルギー	ジュール毎キログラム	J/kg	m^2 s^{-2}
熱伝導率	ワット毎メートル毎ケルビン	W/(m K)	m kg s^{-3} K^{-1}
体積エネルギー	ジュール毎立方メートル	J/m^3	m^{-1} kg s^{-2}
電界の強さ	ボルト毎メートル	V/m	m kg s^{-3} A^{-1}
電荷密度	クーロン毎立方メートル	C/m^3	m^{-3} sA
表面電荷	クーロン毎平方メートル	C/m^2	m^{-2} sA
電束密度，電気変位	クーロン毎平方メートル	C/m^2	m^{-2} sA
誘電率	ファラド毎メートル	F/m	m^{-3} kg^{-1} s^4 A^2
透磁率	ヘンリー毎メートル	H/m	m kg s^{-2} A^{-2}
モルエネルギー	ジュール毎モル	J/mol	m^2 kg s^{-2} mol^{-1}
モルエントロピー，モル熱容量	ジュール毎モル毎ケルビン	J/(mol K)	m^2 kg s^{-2} K^{-1} mol^{-1}
照射線量（X線及びγ線）	クーロン毎キログラム	C/kg	kg^{-1} sA
吸収線量率	グレイ毎秒	Gy/s	m^2 s^{-3}
放射強度	ワット毎ステラジアン	W/sr	m^4 m^{-2} kg s^{-3}=m^2 kg s^{-3}
放射輝度	ワット毎平方メートル毎ステラジアン	$W/(m^2 sr)$	m^2 m^{-2} kg s^{-3}=kg s^{-3}
酵素活性濃度	カタール毎立方メートル	kat/m^3	m^{-3} s^{-1} mol

表５．SI 接頭語

乗数	接頭語	記号	乗数	接頭語	記号
10^{24}	ヨタ	Y	10^{-1}	デシ	d
10^{21}	ゼタ	Z	10^{-2}	センチ	c
10^{18}	エクサ	E	10^{-3}	ミリ	m
10^{15}	ペタ	P	10^{-6}	マイクロ	μ
10^{12}	テラ	T	10^{-9}	ナノ	n
10^{9}	ギガ	G	10^{-12}	ピコ	p
10^{6}	メガ	M	10^{-15}	フェムト	f
10^{3}	キロ	k	10^{-18}	アト	a
10^{2}	ヘクト	h	10^{-21}	ゼプト	z
10^{1}	デカ	da	10^{-24}	ヨクト	y

表６．SIに属さないが、SIと併用される単位

名称	記号	SI 単位による値
分	min	1 min=60s
時	h	1h =60 min=3600 s
日	d	1 d=24 h=86 400 s
度	°	1°=(π/180) rad
分	’	1’=(1/60)°=(π/10800) rad
秒	”	1”=(1/60)’=(π/648000) rad
ヘクタール	ha	$1ha=1hm^2=10^4m^2$
リットル	L，l	$1L=11=1dm^3=10^3cm^3=10^{-3}m^3$
トン	t	$1t=10^3$ kg

表７．SIに属さないが、SIと併用される単位で、SI単位で表される数値が実験的に得られるもの

名称	記号	SI 単位で表される数値
電子ボルト	eV	$1eV=1.602\ 176\ 53(14)\times10^{-19}J$
ダルトン	Da	$1Da=1.660\ 538\ 86(28)\times10^{-27}kg$
統一原子質量単位	u	1u=1 Da
天文単位	ua	$1ua=1.495\ 978\ 706\ 91(6)\times10^{11}m$

表８．SIに属さないが、SIと併用されるその他の単位

名称	記号	SI 単位で表される数値
バール	bar	1 bar=0.1MPa=100kPa=10^5Pa
水銀柱ミリメートル	mmHg	1mmHg=133.322Pa
オングストローム	Å	1 Å=0.1nm=100pm=10^{-10}m
海里	M	1 M=1852m
バーン	b	$1\ b=100fm^2=(10^{-12}cm)2=10^{-28}m^2$
ノット	kn	1 kn=(1852/3600)m/s
ネーパ	Np	SI単位との数値的な関係は、対数量の定義に依存。
ベル	B	
デジベル	dB	

表９．固有の名称をもつCGS組立単位

名称	記号	SI 単位で表される数値
エルグ	erg	$1\ erg=10^{-7}$ J
ダイン	dyn	$1\ dyn=10^{-5}$N
ポアズ	P	1 P=1 dyn s cm^{-2}=0.1Pa s
ストークス	St	1 St =$1cm^2$ s^{-1}=$10^{-4}m^2$ s^{-1}
スチルブ	sb	1 sb =1cd cm^{-2}=10^4cd m^{-2}
フォト	ph	1 ph=1cd sr cm^{-2} 10^4lx
ガル	Gal	1 Gal =1cm s^{-2}=$10^{-2}ms^{-2}$
マクスウェル	Mx	1 Mx = 1G cm^2=10^{-8}Wb
ガウス	G	1 G =1Mx cm^{-2} =10^{-4}T
エルステッド(c)	Oe	1 Oe ≙ $(10^3/4\pi)$A m^{-1}

(c) 3元系のCGS単位系とSIでは直接比較できないため、等号「 ≙ 」は対応関係を示すものである。

表10．SIに属さないその他の単位の例

名称	記号	SI 単位で表される数値
キュリー	Ci	$1\ Ci=3.7\times10^{10}Bq$
レントゲン	R	$1\ R = 2.58\times10^{-4}C/kg$
ラド	rad	$1\ rad=1cGy=10^{-2}Gy$
レム	rem	$1\ rem=1\ cSv=10^{-2}Sv$
ガンマ	γ	$1\ \gamma=1\ nT=10\text{-}9T$
フェルミ		1フェルミ=1 fm=10-15m
メートル系カラット		1メートル系カラット = 200 mg = 2×10-4kg
トル	Torr	1 Torr = (101 325/760) Pa
標準大気圧	atm	1 atm = 101 325 Pa
カロリー	cal	1cal=4.1858J（「15℃」カロリー），4.1868J（「IT」カロリー） 4.184J（「熱化学」カロリー）
ミクロン	μ	1 μ =1μm=10^{-6}m

（第8版，2006年改訂）

この印刷物は再生紙を使用しています